CRYSTAL CHEMISTRY OF SELECTED Sb, As AND P MINERALS

by

Marcus Jason Origlieri

A Dissertation Submitted to the Faculty of the

DEPARTMENT OF GEOSCIENCES

In Partial Fulfillment of the Requirements
For the Degree of

DOCTOR OF PHILOSOPHY

In the Graduate College

THE UNIVERSITY OF ARIZONA

2005

THE UNIVERSITY OF ARIZONA
GRADUATE COLLEGE

As members of the Dissertation Committee, we certify that we have read the dissertation prepared by Marcus Jason Origlieri

entitled Crystal Chemistry of Selected Sb, As, and P Minerals

and recommend that it be accepted as fulfilling the dissertation requirement for the Degree of Doctor of Philosophy

_____ Date: November 15, 2005
Robert T. Downs

_____ Date: November 15, 2005
M. Bonner Denton

_____ Date: November 15, 2005
Mihai N. Ducea

_____ Date: November 15, 2005
Charles T. Prewitt

Final approval and acceptance of this dissertation is contingent upon the candidate's submission of the final copies of the dissertation to the Graduate College.

I hereby certify that I have read this dissertation prepared under my direction and recommend that it be accepted as fulfilling the dissertation requirement.

_____ Date: November 15, 2005
Dissertation Director: Robert T. Downs

STATEMENT BY AUTHOR

This dissertation has been submitted in partial fulfillment of requirements for an advanced degree at the University of Arizona and deposited in the University Library to be made available to borrowers under rules of the Library.

Brief quotations from this dissertation are allowable without special permission, provided that accurate acknowledgment of source made. Requests for permission for extended quotation from or reproduction of this manuscript in whole or in part may be granted the head of the major department or the Dean of the Graduate College when in his or her judgment the proposed use of the material is in interests of scholarship. In all other instances, however, permission must be obtained from the author.

SIGNED: _____

Marcus Origlieri

DEDICATION

I thank Richard A. Bideaux for the inspiration to undertake these studies

TABLE OF CONTENTS

LIST OF TABLES

LIST OF FIGURES

ABSTRACT

The crystal structures of the related minerals triploidite (Mn_2PO_4OH) and zwieselite (Fe_2PO_4OH) are discussed. Order-disorder of OH^- and F^- in these structures is discussed using the results of new crystal structure refinements, and correlation with the results of Raman spectroscopic study in the hydroxyl stretching region. Cryogenic crystal structure refinement of triploidite allowed the distinction of separate OH^- and F^- sites in the mineral.

A new mineral, natural $AsSbO_3$, has been found at Tsumeb, Namibia. Its occurrence has implications on the closing stage of ore formation at this mine. The crystal structure has been solved, and shown to have long range As-O and Sb-O bonding using electron density distributions from quantum calculations.

INTRODUCTION

Since my youth, I have studied minerals with every available technique. I chose graduate school in mineralogy to understand crystallography using current technology and modern theory. Minerals have long geologic histories, and many have interesting stories. Among the many samples brought to my attention, one, occurring as bright red transparent masses from China, was the phosphate triploidite (Mn_2PO_4OH). Standardized microprobe analysis demonstrated a formula consistent with triploidite, however the powder X-ray diffraction pattern showed some differences. This triploidite has C2/c symmetry, which is more symmetric than $P2_1/c$ Connecticut material. This study indicates that disorder of F^- and OH^- within a single crystallographic results in a greater symmetry. In order to better understand the nature of ordering of F^- and OH^- in this structure type, the related mineral zwieselite (Fe_2PO_4F) was studied with single crystal X-ray diffraction and Raman spectroscopy. The results suggest a model with two separate crystallographic sites: one preferentially fills with F^- and the other accommodates both F^- and OH^-. Together, these two papers clarify the crystal chemistry of the triplite-triploidite group of minerals of general formula $M_2(PO_4)X$.

Another mineral caught my attention, as lustrous bladed crystals associated with the rare arsenic mineral leiteite. These crystals proved to be natural $AsSbO_3$, which is a new mineral. A descriptive paper discusses the nature of the discovery and implication for the geochemistry of the Tsumeb mine. And another paper includes the crystal

structure solution, with corner linked AsO_3 and SbO_3 groups forming infinite sheets. The sheets of the structure showed a pronounced corrugation, which stems from extended As-O interaction over 3 Å. The new mineral is compared with the isostructural mineral claudetite, and new structural data with anisotropic displacement parameters are presented for that mineral as well. In this study, scrutiny of the bonding associated with AsO_3 and SbO_3 groups shows many extended metal-oxygen interactions. These extended metal - oxygen interactions lead to polymerization of AsO_3 and SbO_3 in minerals, and have implications pertinent to the toxicity of As^{3+} and Sb^{3+}.

PRESENT STUDY

Two crystallographically related phosphate minerals, triploidite and zwieselite share the same space group symmetry. Triploidite is a manganese phosphate hydroxide detailed in Appendix A while zwieselite is an iron phosphate fluoride as shown in Appendix B. X-ray diffraction methods, detailed in appendices A and B, afforded high precision models of these crystal structures. These two minerals have corresponding cation positions, but the bonding coordination of these sites varies between the minerals. The bonding differences are related to positions of the hydroxide and fluorine in the structure. Spectroscopic evidence indicates that all of the OH^- in these structures fits into a single crystallographic site. In conclusion, four metal atoms coordinate to each fluorine atom, while hydroxide ions coordinate to only three metal atoms.

A new mineral has been discovered at Tsumeb, Namibia, and found to be the natural equivalent of synthetic $AsSbO_3$. Appendix 3 describes the properties of the new mineral, as gathered from the methods of X-ray diffraction, Raman spectroscopy, and electron microprobe analysis. Appendix D reports the solution of the crystal structure from X-ray diffraction data, and the results of ab initio quantum modeling of the crystal structure. The structure is related to the mineral claudetite and the differences between the bonding of Sb and As are related.

APPENDIX A

ORDER-DISORDER OF F^- AND OH^- IN THE CRYSTAL STRUCTURE OF ZWIESELITE

Marcus J. Origlieri[1*]

Robert T. Downs[1§]

Tom A. Laetsch[1]

[1]Department of Geosciences, University of Arizona, Tucson, Arizona 85719–0077 USA

*marcus@geo.arizona.edu; §downs@geo.arizona.edu

Abstract

We have refined the crystal structure of zwieselite from the Cornelia mine, Hagendorf, Germany. Zwieselite is monoclinic, space group C2/c, a = 13.2543(8) Å, b = 6.5092(4) Å, c = 10.0143(7) Å, β = 119.255(3)°, V = 753.78(8) $Å^3$ and Z = 8, with empirical formula $(Fe^{2+}_{1.041}Mn_{0.861}Fe^{3+}_{0.029}Ca_{0.056}Mg_{0.007}Ti^{4+}_{0.004}Zn_{0.004})_{\Sigma=2}$ $(P_{0.978}Si_{0.009}Fe^{3+}_{0.009}Al_{0.004})_{\Sigma=1}$ O_4 $(F_{0.850}OH_{0.150})_{\Sigma=1}$. Zwieselite is a member of a large group of minerals with chemistry $M_2(TO_4)X$, including wolfeite, triplite and triploidite. The structure has two distinct transition metal sites, and one phosphorus site. There are five symmetrically unique anion sites, four of which complete the phosphate tetrahedron and are fully occupied by oxygen. A fifth site contains both F^- and OH^-. Refining the F^-/OH^- position as a single site yielded a large displacement ellipsoid. The refinement was improved by splitting this single site into two nonequivalent sites separated by 0.388 Å with a total occupancy of 1 F^-/OH^-. One of these sites coordinates with four metal atoms, while the other site coordinates with only three metal atoms. By comparison with the wolfeite and triploidite structures, we conclude that only F^- occupies the four-coordinated anion site, while both F^- and OH^- anions occupy the three-coordinated site. Raman spectroscopic data shows a single OH^- stretching peak in the OH^- stretching region, indicating that the entire OH^- content resides in only one of the two split site positions.

Introduction

Breithaupt (1841) originally assigned the name zwiselite [sic] to a phosphate of iron and manganese from near Zwiesel, Bavaria. Glocker (1847) introduced the name zwieselite to match the proper spelling of the locality. In the seventh edition of Dana's System of Mineralogy, Palache et al. (1949) listed zwieselite within the description of triplite (Mn_2PO_4F), not distinguishing the mineral as a separate species. The mineral achieved species status in the interim, as Mandarino and Back (2004) report the idealized formula $Fe_2(PO_4)F$ for zwieselite and further note a solid solution with triplite.

Synthetic $Fe_2(PO_4)F$ has been characterized by single crystal diffraction (Yakubovich et al. 1978). The crystal structure has one unique phosphorus location, in a typical PO_4 tetrahedron, and two nonequivalent Fe sites, each coordinated with 4 O and 2 F atoms. The crystal structure consists of these distorted octahedra linked in an edge sharing open framework crosslinked with corner sharing PO_4 groups. The refined fluorine site exhibited a large anisotropic displacement ellipsoid.

Zwieselite is a member of a large group of similar phosphate minerals, including triplite and its hydroxyl analog triploidite (Mn_2PO_4OH). The crystal structures of triplite and triploidite are closely related but not isostructural. The crystal structure of triplite was solved in space group $I2/a$ by splitting a fluorine site into two half occupied fluorine sites at a separation of 0.62 Å (Waldrop, 1969). Waldrop (1970) chose a unit cell for triploidite with a b-axis double that of triplite, attributing this choice to ordering of OH^-

into one of the two split sites of the triplite structure. The ordering of the OH^- in the triploidite structure resulted in a lowering of space symmetry to $P2_1/a$. Yakubovich et al. (1978) solved synthetic Fe_2PO_4F in $I2/a$, choosing a unit cell dimensionally related to triplite, however solving the F in one site. A new structure determination of zwieselite has been initiated to investigate the proper unit cell and structure of the mineral.

Experimental

Qualitative WDS scans on an epoxy grain mount of zwieselite from the Cornelia mine, Hagendorf, Germanythat showed major Fe, Mn, P, F and minor Mg, Ca, and F. Standardized analysis employed a Cameca SX-50 electron microprobe in quantitative WDS mode. Operating conditions were 15 kV and 40 nA with a beam diameter of 1.5 µm. Albite (Al), diopside (Mg, Si, Ca), MgF_2 (F), apatite (P), rutile (Ti), and fayalite (Fe), rhodonite (Mn), and $ZnFe_2O_4$ spinel (Zn) served as standards. Data reduction and correction followed the PAP method (Pouchou & Pichoir 1984, 1985). Table 1 presents the average of 15 microprobe spot analyses. The analyses were normalized to three total cations, assuming occupancy of 1 ($F^- + OH^-$) per formula unit, and adjusting Fe^{3+}/Fe^{2+} to achieve charge balance.

From a fragment of zwieselite from the Cornelia mine, Hagendorf, Germany, we collected single crystal diffraction data using a Bruker X8 Apex diffractometer equipped with a 4K Apex II CCD detector with monochromatic MoKα radiation generated at 50 kV and 35 mA. We used the Bruker Apex2 software package for absorption corrections

and scaling the data. The initial structure solution used direct methods (Sheldrick, 1990). Subsequent refinement of the structure employed Shelx97 (Sheldrick 1997). XTALDRAW software rendered the crystal structure for viewing and generation of figures. METRIC97 (Bartelmehs et al. 1993) software confirmed bond lengths and angles. Details of the refinement are in Table 2.

We collected Raman spectra of the OH^- stretching region using an Nicolet AlmegaXR Dispersive Raman microscope with a 532 nm laser wavelength and a 2400 groves mm^{-1} grating. Thermo Corporation OMNIC 7.1 software to collected spectrum from a Peltier-cooled 1024 × 256 pixel CCD.

Crystal Structure Solution

The crystal structure was solved using direct methods, locating 1 P and 2 Fe atoms. Oxygen atoms were added to complete a tetrahedral arrangement for the phosphate group, and a fluorine atom was located between Fe atoms. The Fe, P, and O atoms refined with anisotropic displacement parameters typical of PO_4 and Fe in $Fe(\phi)_6$ groups. The F atom displayed a quite elongated displacement ellipsoid. This refinement cycle gave an R1 value of 2.69%. In order to improve the structural model, the F location was split into two sites, denoted F1 and F2. They were assigned occupancies of 0.85 and 0.15, to achieve a total occupancy of 1 (F + OH). Splitting the F location dropped R1 to the final value of 2.26% over all reflections. The structure solution is given in Table 3.

Previous structure solutions for minerals of the triplite and triploidite groups have used space group symmetries I2/a (Waldrop, 1969; Yakubovich et al. 1978; Tadini, 1981; Kolitsch, 2003) and $P2_1/a$ (Waldrop, 1970), respectively. Rea and Kostiner (1972) alternately solved synthetic Mn_2PO_4F in C2/c, whose setting we have followed.

Yakubovich et al. (1978) solved the crystal structure of synthetic end-member zwieselite ($Fe_2(PO_4)F$) in the space group I2/a. A notable feature of their structure is the large displacement ellipsoid for the F atom, statistically identical to the refined values of our F1 site. The F1 site in our structural model has coordination number associated with two M1 atoms at 2.083 Å and 2.522 Å and two M2 atoms at 2.088 Å and 2.460 Å. Figure 2 shows the coordination of F1. Because of its larger refined occupancy and the dominance of F in empirical chemistry, we conclude that the F1 site is occupied by 0.85 F per formula unit.

The OH^- chemical analog of zwieselite, wolfeite (Kolitsch, 2003) shows a doubled **b** cell edge. Ordering of the OH^- in the structure lowers the symmetry from I2/a (C2/c in our setting) to $P2_1/a$. The F2 ellipsoid in zwieselite occupies the volume between the two separate O17 and O18 positions in wolfeite (Kolitsch, 2003). In zwieselite, F2 coordinates to three atoms: one M1 at 2.119 Å and two M2 at 2.022 Å and 2.258 Å, as shown in Figure 3. Due to its lower refined occupancy than the F1 site, and the minor OH^- content of the mineral, we conclude that this site is occupied by OH^-.

Zwieselite and wolfeite have similar crystal structures, but are not isotypic. The definition of isotypic relationship given by the IuCR (J. Lima-de-Faria et al. 1990)

requires in addition to having similar positions in a similar unit cell, similar atoms must also have similar chemical bonding relationships to qualify as isotypic. In fluorine dominant Fe_2PO_4F, fluorine resides in a four coordinated site, while in an OH^- dominant Fe_2PO_4OH, OH^- resides in a three coordinated position.

Raman spectrum

The Raman spectrum of the OH^- stretching region showed only a single, weak peak centered at 3498 rel. cm^{-1}. The Raman spectrum of the OH^- spectrum of wolfeite (Fe_2PO_4OH) shows multiple peaks (Kolitsch, 2003) with an average position of 3518 rel. cm^{-1}. Wolfeite is closely related to zwieselite, with a unit cell doubled along b, caused by the splitting of the OH^-/F^- site into two nonequivalent sites, neither of which are simultaneously occupied, with a corresponding symmetry reduction from $I2/a$ to $P2_1/a$. The single peak in our OH^- stretching region could be from a single bond, especially one with a large thermal displacement parameter, or from many distinct peaks of very similar energies from that portion of the crystal structure. Based on comparison with the wolfeite spectrum, it is clear that the OH^- does not occupy both of the split sites, but only occupies one of them. Given the broad nature of the peak in the zwieselite spectrum, as seen in figure 4, it likely represents the split F site with the larger thermal displacement parameter, namely F2.

References

Breithaupt (1841) Vollständiges Handbuch der Mineralogie. Band II. Dresden.

Glocker (1847) Generum et specierum mineralium secundum ordines naturales digestorum synopsis. Halle.

Kolitsch, U. (2003) Mg-rich wolfeite, $(Fe^{II},Mg)_2(PO_4)(OH)$: structure refinement and Raman spectroscopic data. Acta Crystallographica, E59, 126–128.

Lima de Faria, J., E. Hellner, F. Liebau, E. Makovicky, and E. Parthé (1990) Nomenclature of inorganic structure types. Acta Crystallographica, A46, 1–11.

Mandarino, J.A. and M.E. Back (2004) Fleischer's glossary of mineral species 2004. The Mineralogical Record, Inc., Tucson, Arizona. 309 pp.

Palache, C., H. Berman and C. Frondel (1951) Dana's System of Mineralogy. Seventh edition. Volume II. John Wiley and Sons, New York. Pages 849–852.

Pouchou, J.L. and Pichoir, F. (1984) Un nouveau modèle de calcul pour la microanalyse quantitative par spectrométrie de rayons X. Partie I: Application a l'analyse d'énchantillons homogènes. La Recherche Aérospatiale, number 3, 167–192.

Pouchou, J.L. and F. Pichoir (1985) "PAP" $\phi(\rho Z)$ procedure for improved quantitative microanalysis. In Armstrong, J.T. ed. (1985) Microbeam Analysis 1985, San Francisco Press, 104–106.

Rea, J.R. and E. Kostiner (1972) The crystal structure of manganese fluorophosphate, $Mn_2(PO_4)F$. Acta Crystallographica, B28, 2525–2529.

Tadini, C. (1981) Magniotriplite: its crystal structure and relation to the triplite-triploidite group. Bulletin de Minéralogie, 104, 677–680.

Waldrop, L. (1969) The crystal structure of triplite. Zeitschrift für Kristallographie, 130, 1–14.

Waldrop, L. (1970) The crystal structure of triploidite and its relations to the structures of other minerals of the triplite-triploidite group. Zeitschrift für Kristallographie, 131, 1–20.

Yakubovich, O.V., M.A. Simonov, E.N. Matvienko, and N.V. Belov (1978) The crystal structure of the synthetic Fe end member of the series triplite – zwieselite $Fe_2(PO_4)F$, space group I2/a. Doklady Akademii Nauk SSSR 238, 576–579 (in Russian).

Table 1. Average of fifteen spot microprobe analysis of zwieselite. Normalized to three total cations, and charge balancing by adjusting Fe^{3+}/Fe^{2+} yields the empirical formula $(Fe^{2+}_{1.041}Mn_{0.861}Fe^{3+}_{0.029}Ca_{0.056}Mg_{0.007}Ti^{4+}_{0.004}Zn_{0.004})_{\Sigma=2}$ $(P_{0.978}Si_{0.009}Fe^{3+}_{0.009}Al_{0.004})_{\Sigma=1}$ O_4 $(F_{0.850}OH_{0.150})_{\Sigma=1.}$ H_2O was assumed to achieve 1 (F^- + OH^-) per formula unit.

Al_2O_3	0.09%
SiO_2	0.35%
F	7.11%
MgO	0.13%
P_2O_5	30.54%
CaO	1.39%
TiO_2	0.23%
MnO	26.88%
FeO	34.05%
ZnO	0.15%
–O=2F	-3.00%
H_2O	[1.16%]
sum	[99.08%]

Table 2. Crystal structure refinement parameters for zwieselite.

space group	*C*2/*c*
a	13.2543(8) Å
b	6.5092(4) Å
c	10.0143(7) Å
β	119.255(3)°
V	753.78(8) $Å^3$
Z	8
refined chemistry	$(Fe_{0.58}Mn_{0.35}Ca_{0.07})(Fe_{0.50}Mn_{0.50})(PO_4)(F_{0.85}OH_{0.15})$
empirical chemistry	$(Fe^{2+}_{1.041}Mn_{0.861}Fe^{3+}_{0.029}Ca_{0.056}Mg_{0.007}Ti^{4+}_{0.004}Zn_{0.004})_{\Sigma=2}$ $(P_{0.978}Si_{0.009}Fe^{3+}_{0.009}Al_{0.004})_{\Sigma=1}\ O_4\ (F_{0.850}OH_{0.150})_{\Sigma=1}$
calc. density	3.939 g/cm^3
T	298 K
crystal size	110 × 100 × 70 µm
maximum 2θ	103°
total reflections	3864
obs refl. ($F > 4\sigma$)	3514
index range	−28 = h = 28 −13 = k = 11 −21 = l = 18
R_{sym}	2.06%
R_{obs}	2.26%
R_{all}	2.58%
GooF (overall)	1.074

Table 3. Atomic coordinates and atomic displacement parameters for zwieselite.

site	x	y	z	Uiso	U11	U22	U33	U12	U13	U23
M1	0.05693(1)	0.26774(2)	0.99861(1)	0.01188(3)	0.01083(4)	0.01423(6)	0.01080(4)	0.00380(3)	0.00547(3)	0.00223(3)
M2	0.34280(1)	0.39660(2)	0.64537(1)	0.01067(2)	0.01358(4)	0.00779(5)	0.01139(4)	-0.00067(3)	0.00669(3)	0.00029(3)
P	0.17496(1)	0.40694(3)	0.80561(2)	0.00694(3)	0.00678(5)	0.00606(7)	0.00675(6)	0.00013(4)	0.00235(5)	0.00005(5)
O1	0.30634(6)	0.08244(10)	0.58157(7)	0.0122(1)	0.0164(2)	0.0085(2)	0.0099(2)	-0.0009(2)	0.0050(2)	0.0021(2)
O2	0.21092(5)	0.14265(11)	0.19228(7)	0.0128(1)	0.0102(2)	0.0170(3)	0.0128(2)	0.0040(2)	0.0068(2)	0.0025(2)
O3	0.41818(5)	0.03542(11)	0.35749(7)	0.0128(1)	0.0117(2)	0.0130(3)	0.0082(2)	-0.0005(2)	0.0005(1)	0.0021(2)
O4	0.36773(5)	0.28172(10)	0.14229(8)	0.0119(1)	0.0129(2)	0.0079(2)	0.0149(2)	-0.0014(1)	0.0069(2)	0.0014(2)
F1	0.0180(2)	0.0954(3)	0.3972(2)	0.0290(4)	0.0228(6)	0.0241(6)	0.0476(10)	-0.0042(4)	0.0232(7)	-0.0151(5)
F2	0.0100(7)	0.1431(20)	0.3651(13)	0.034(3)	0.005(1)	0.053(8)	0.032(4)	-0.005(3)	0.000(2)	-0.036(5)

notes:
M1 = $Fe_{0.58}Mn_{0.35}Ca_{0.07}$
M2 = $Fe_{0.50}Mn_{0.50}$
F1 = $F_{0.85}$
F2 = $OH_{0.15}$

Table 4. Selected bond lengths (Å) and angles for zwieselite.

M1-F1	2.083(2)	M2-O2	2.085(1)
M1-O4	2.114(1)	M2-F1	2.088(2)
M1-O3	2.117(1)	M2-O4	2.122(1)
M1-O2	2.173(1)	M2-O1	2.127(1)
M1-O3	2.181(1)	M2-O1	2.168(1)
M1-F1	2.522(2)	M2-F1	2.460(1)
M1-F2	2.12(1)	M2-F2	2.26(1)
		M2-F2	2.02(1)
P-O1	1.5392(7)		
P-O2	1.5369(6)		
P-O3	1.5367(6)		
P-O4	1.5456(7)		
<<O-P-O>	109.47(4)°		

Figure 1. View of the structure of zwieselite down b. The M1 and M2 polyhedra are coordinated by O and F1 atoms only. Fluorine atoms were split into two nearby sites, listed as F1 and F2 in Table 3.

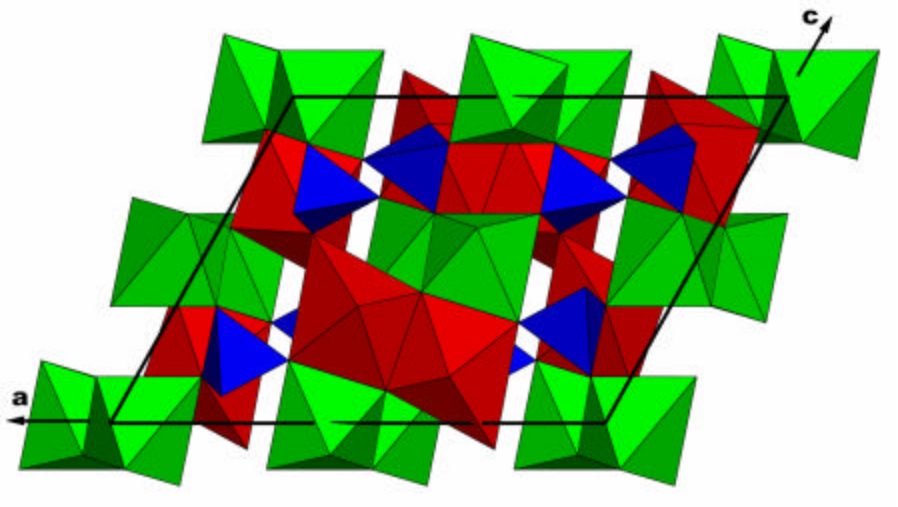

Figure 2. View of the coordination of the F1 ellipsoid, drawn at 99% probability, using the same scale and orientation as Figure 1. F1 coordinates to M1 at 2.083 Å and 2.088 Å, and also to M2 at 2.522 Å and 2.460 Å. The F1 site is populated by fluorine atoms (0.85 apfu) coordinated to the four nearby metal atoms.

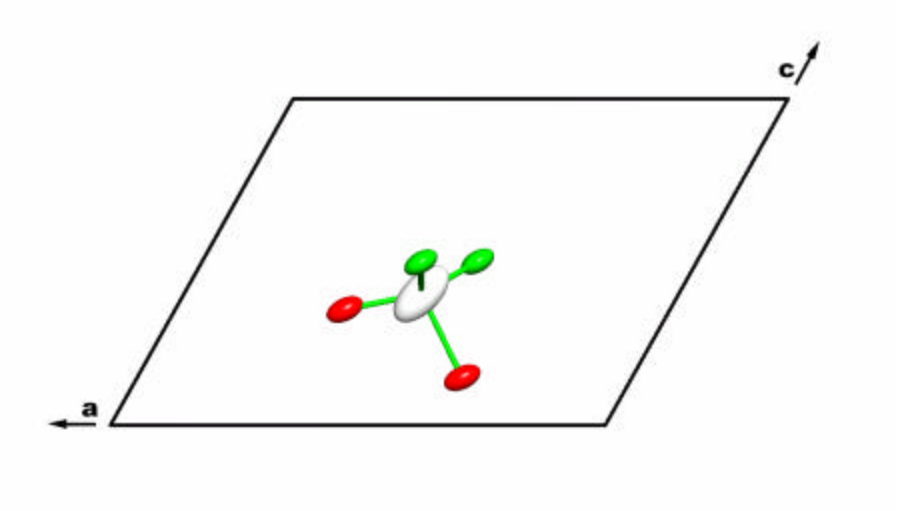

Figure 3. View of the coordination of the F2 ellipsoid, viewed down b using the same scale and orientation as Figure 1. The F2 site is 2.022 Å and 2.258 Å from M2 sites, and 2.119 Å from M1. The next nearest M1 atom has a separation of 2.880 Å. This site would preferentially take OH^- ions, since it has fewer bonded interactions than the F1 site. Spectroscopic evidence presented in Figure 4 indicates only one Raman active mode in zwieselite, which indicates that all OH^- orders into a single crystallographic site.

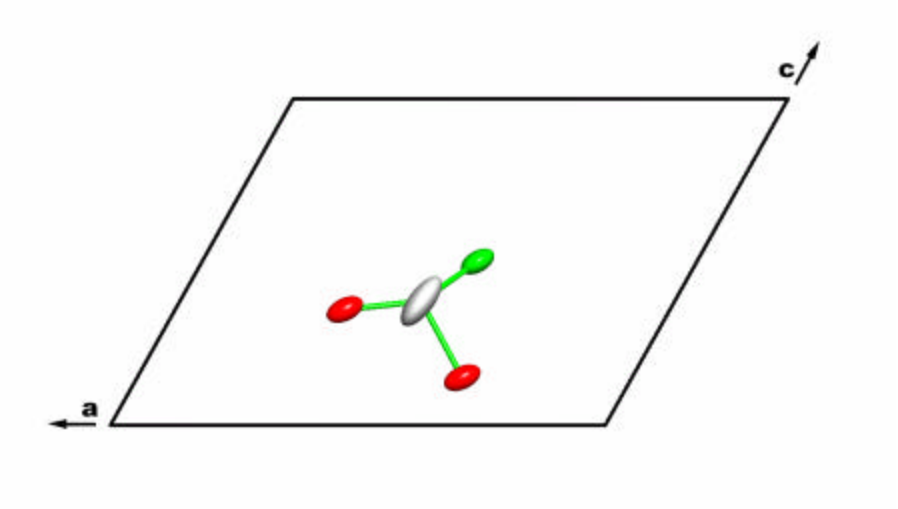

Figure 4. Raman spectrum in the OH^- stretching region of zwieselite, showing a single broad peak centered at 3498 shifted cm^{-1}. The single mode indicates the OH^- occupies a single location in the crystal structure, and its broad nature is consistent with the large thermal parameter of the F2 site as listed in Table 3. Figure 3 shows the coordination of the F2 site.

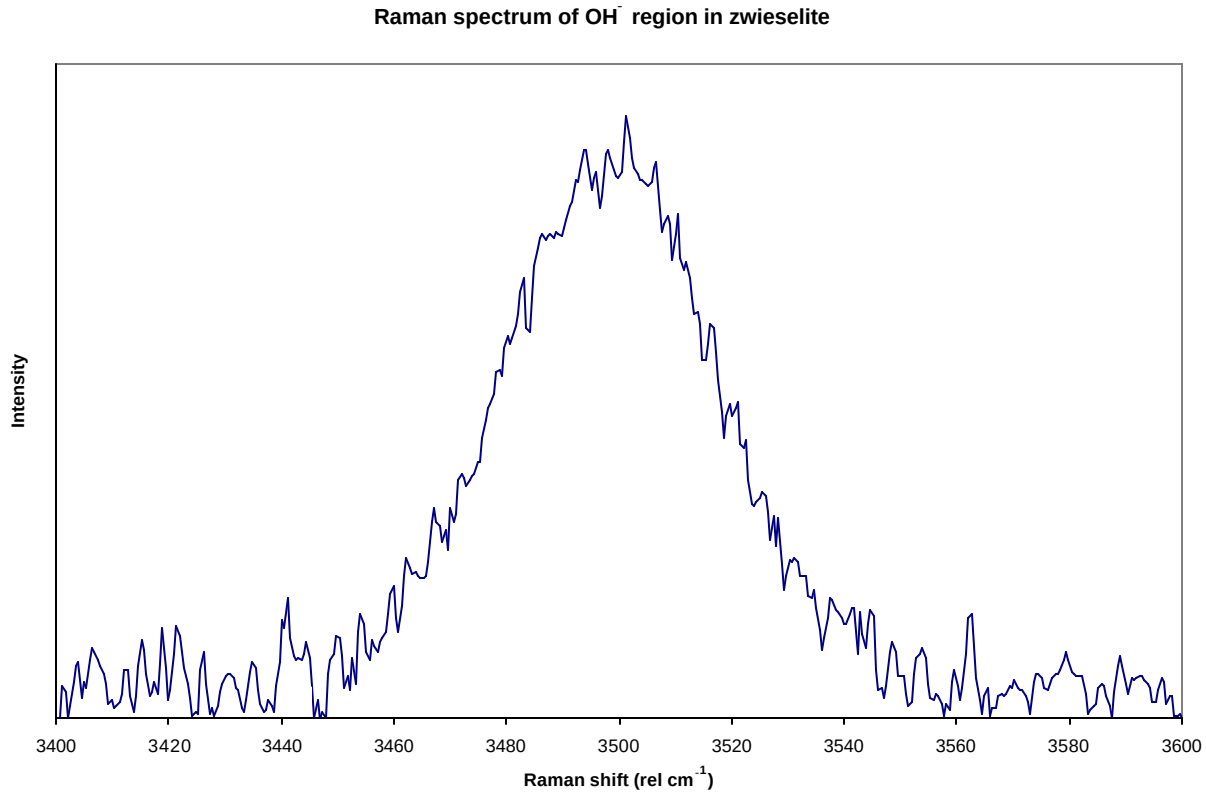

APPENDIX B

THE CRYSTAL STRUCTURE OF TRIPLOIDITE SOLVED IN THE SPACE GROUP OF TRIPLITE.

Marcus J. Origlieri[1*]

Robert T. Downs[1§]

John C. Lucking[2]

[1]Department of Geosciences, University of Arizona, Tucson, Arizona 85721–0077 USA

[2]7537 North Central Avenue, Phoenix, Arizona 85020 USA

*marcus@geo.arizona.edu; §downs@geo.arizona.edu

Abstract

Single crystal X-ray study of triploidite from a new occurrence in China shows monoclinic symmetry, C2/c, with lattice parameters a = 13.3611(4) Å, b = 6.4923(2) Å, c = 10.0611(3) Å, β = 119.818(1)°, V = 757.20(4) $Å^3$, Z = 8. The empirical formula from microprobe is $(Mn_{1.701}Mg_{0.153}Fe^{3+}_{0.054}Fe^{2+}_{0.051}Ca_{0.041})_{\Sigma=2}(P_{0.973}Fe^{3+}_{0.027})_{\Sigma=1}O_4(OH_{0.666}F_{0.334})_{\Sigma=1}$. Previous structure refinements of Connecticut material have shown $P2_1/c$ symmetry in this phase. This material shows additional symmetry afforded by complete disorder of the OH/F in the structure. Raman spectroscopy indicates that all of OH^- content of the mineral falls into a single crystallographic site. Cryogenic refinement allowed the resolution of a large thermal ellipsoid into two separate sites, one occupied with OH^- and the other occupied by F^-.

Introduction

Following the Tucson Mineral Show of 2005, mineral collector John Lucking showed an interesting bright red mineral to one of the authors (MJO). The bright red color resembles that of gem quality rhodonite, and consequently the phase was assumed to have essential manganese. Initial study by powder X-ray diffraction failed to find a suitable match. The mineral gave an intense and sharp Raman spectrum.

One of the authors (JCL) purchased this mineral in China, but could not obtain reliable locality information at that time. The mineral occurs with pyrite, sphalerite, and quartz. This assemblage likely originates from a hydrothermal system. The mineral is hydroxyl dominant, indicating that the occurrence is relatively fluorine poor. A probable locality for this mineral is Daoping manganese deposit.

Subsequent microprobe analysis indicated a formula near $Mn_2(PO_4)(OH,F)$. Triploidite has such a formula, however our observed powder pattern did not match published patterns for triploidite. However, the pattern resembled triplite, which is a fluorine dominant and near structural analog of triploidite. These two minerals are members of a sizable group of minerals, listed in Table 1. Waldrop (1970) indicates that triploidite and triplite, though differing by only substitution of F for OH, are not isotypic. They have different unit cell dimensions and space groups. In this paper, we report the powder pattern, chemistry, and single crystal structure analysis of another triploidite.

Experimental

We used an epoxy mount of a triploidite grain for microprobe analysis. A qualitative WDS scan showed major Mn, Fe, P, and minor Mg, Ca, and F. Standardized WDS analysis employed a Cameca SX-50 in quantitative WDS mode. Operating conditions were 15 kV and 40 nA with a beam diameter of 1.5 μm. Apatite (Ca, F, P), diopside (Mg), rhodonite (Mn) and fayalite (Fe) served as standards. Data reduction and correction followed the PAP method (Pouchou & Pichoir 1984, 1985). Table 2 presents the average of 50 microprobe spot analyses.

We collected X-ray powder diffraction data on a Bruker D8 Advance in the Department of Geosciences, University of Arizona. Data were collected using CuKα radiation between 5 and 90 degrees 2θ, using CuKα radiation generated at 40 kV and 40 mA. We refined the unit cell dimensions using inhouse software. The initial indexing followed the unit cell reported by Rea and Kostiner (1972). The X-ray powder diffraction pattern constitutes Table 3.

A Bruker X8 Apex diffractometer equipped with a 4K Apex II CCD detector served to study the X-ray diffraction patterns using monochromatic MoKα radiation generated at 50 kV and 35 mA. A crystal fragment of $160 \times 120 \times 50$ μm gave sharp diffraction spots. We performed two separate data collections, the first at room temperature, and the second at 100 K. The purpose of the second data collection was to determine whether a large displacement ellipsoid observed in the room temperature

refinement persisted, which would distinguish order-disorder from thermal motion. Table 4 lists the details of the refinements.

In order to determine the nature of the large anisotropic displacement parameter, teh triploidite was studied at 100 K. A stream of cold dry air was gemerated with a Cryosystems Kryoflex machine. Absorption corrections and scaling used the Bruker Apex2 software package. The initial structure solution used direct methods (Sheldrick, 1990). Subsequent refinement of the structure employed Shelx97 (Sheldrick 1997). XTALDRAW software rendered the crystal structure for viewing and generation of figures. METRIC97 (Bartelmehs et al. 1993) software allowed confirmation of bond lengths and angles.

Raman spectroscopy employed a benchtop Ar-ion laser centered at 514.532 nm with a power output of 100 mW. A Jobin Yvon Spex HR 460 spectometer and a liquid nitrogen cooled Princeton Instruments 1152×256 pixel CCD detector. Using a grating with 1200 groves mm^{-1} centered at 530.4 nm, Roper Instruments Winspec/32 software collected the shifted region from 113 to 1016 cm^{-1}.

Crystal Structure Solution & Discussion

The room conditions crystal structure was solved using direct methods, locating 2 Mn and 1 P atom. Oxygen atoms were added to complete a tetrahedral arrangement for the P atom and another oxygen atom was located between Mn atoms. A fifth peak, equivalent to the other oxygen atoms in magnitude, was assigned as OH, and refined

using the fluorine scattering factor. Utilizing the neutral O atom scattering factor increased the value of R by 0.5%. The implication of this refinement behavior was assumed to indicate additional electron density of a hydrogen attached to the oxygen atom. Unfortunately, the hydrogen could not be located in the refinement. Upon the final refinement, the unit cell settings of Rea and Kostiner (1972) were followed.

In order to locate the hydrogen atom, a cryogenic refinement was undertaken. Unfortunately, the hydrogen could not be located empirically. The displacement ellipsoid of the OH^- site was reduced by about 35%. The volume of the OH^- displacement ellipsoid scaled to a smaller extent than those of the O atoms from Tables 5 and 6, which are 50% smaller. This behavior of the displacement ellipsoid to remain relatively large compared to others indicates a disorder condition for the crystallographic site.

The OH^- position in the triploidite matches the F^- position in triplite (Mn_2PO_4F) by Rea and Kostiner (1972) and corresponds the F(av) position in Waldrop (1969). Waldrop (1970) solved the crystal structure of triploidite in $P2_1/c$ by splitting the single F site into two positions, and doubling the unit cell edge.

References

Anthony, J.W., R.A. Bideaux, K.W. Bladh and M.C. Nichols (2000) Handbook of mineralogy. Volume IV. Arsenates, phosphates, vanadates. Mineral Data Publishing, Tucson, Arizona. 680 pp.

Pouchou, J.L. and Pichoir, F. (1984) Un nouveau modèle de calcul pour la microanalyse quantitative par spectrométrie de rayons X. Partie I: Application a l'analyse d'énchantillons homogènes. La Recherche Aérospatiale, number 3, 167–192.

Pouchou, J.L. and F. Pichoir (1985) "PAP" $\phi(\rho Z)$ procedure for improved quantitative microanalysis. In Armstrong, J.T. ed. (1985) Microbeam Analysis 1985, San Francisco Press, 104–106.

Rea, J. R. and E. Kostiner (1972) The crystal structure of manganese fluorophosphate, $Mn_2(PO_4)F$. Acta Crystallographica, B28, 2525–2529.

Waldrop, L. (1969) The crystal structure of triplite. Zeitschrift für Kristallographie, 130, 1–14.

Waldrop, L. (1970) The crystal structure of triploidite and its relations to the structures of other minerals of the triplite-triploidite group. Zeitschrift für Kristallographie, 131, 1–20.

Table 1. Known minerals of the triplite and triploidite groups, after Anthony et al. (2004).

	chemistry	symmetry	a	b	c	β	Z
isokite	$CaMg(PO_4)F$	C2/c	6.52	8.75	7.51	121.47	4
magniotriplite	$(Mg,Fe,Mn)_2(PO_4)(F,OH)$	I2/a	12.035	6.432	9.799	108.12	8
panasqueiraite	$CaMg(PO_4)(OH,F)$	C2/c	6.535	8.753	6.919	112.33	4
sarkinite	$Mn_2(AsO_4)(OH)$	$P2_1/a$	12.779	13.596	10.208	108.88	16
triplite	$(Mn,Fe,Mg,Ca)_2(PO_4)(F,OH)$	I2/a	12.065	6.454	9.937	107.09	8
triploidite	$(Mn,Fe)_2(PO_4)(OH)$	$P2_1/a$	12.366	13.276	9.943	108.23	16
wagnerite	$(Mg,Fe)_2(PO_4)F$	$P2_1/a$	11.945	12.679	9.644	108.18	16
wolfeite	$(Fe,Mn)_2(PO_4)(OH)$	$P2_1/a$	12.319	13.230	9.840	108.40	16
zwieselite	$(Fe,Mn)_2(PO_4)F$	$I2/a$	12.085	6.536	9.910	105.63	8

Table 2. Average of 50 microprobe analyses with standard deviations for triploidite. Normalized to three total cations, assuming full occupancy of the sites and charge balancing OH^- and Fe^{3+}/Fe^{2+}, the empirical formula is $(Mn_{1.701}Mg_{0.153}Fe^{3+}_{0.054}Fe^{2+}_{0.051}Ca_{0.041})_{\Sigma=2}$ $(P_{0.973}Fe^{3+}_{0.027})_{S=1}\ O_4\ (OH_{0.666}F_{0.334})_{S=1}$.

MnO	55.83(0.83)
MgO	2.83(0.28)
FeO	4.34(1.07)
CaO	1.05(0.08)
P_2O_5	31.68(0.34)
F	2.91(0.12)
–O=2F	1.22
H_2O	[2.75]
total	[100.17]

Table 3. X-ray powder diffraction pattern of triploidite.

2theta	d	h	k	l
24.357	3.66756	-3	1	1
24.419	3.66744	-3	1	1
27.259	3.28177	-4	0	2
27.328	3.28174	-4	0	2
29.433	3.04322	0	2	1
29.508	3.04317	0	2	1
31.668	2.83261	2	2	0
31.749	2.83256	2	2	0
34.495	2.60592	0	2	2
34.583	2.60593	0	2	2
35.696	2.52068	2	2	1
35.788	2.52064	2	2	1
36.123	2.49177	-2	0	4
36.216	2.49174	-2	0	4
42.878	2.11254	-1	3	1
42.990	2.11252	-1	3	1
44.648	2.03261	-6	0	4
44.765	2.03260	-6	0	4
47.084	1.93273	6	0	0
47.208	1.93272	6	0	0
50.903	1.79601	-1	1	5
51.038	1.79601	-1	1	5

Table 4. Unit cell data for triploidite from single crystal data.

	room condition (single F site)	cryogenic (single F site)	cryogenic (split F sites)
space group	*C*2/*c*	*C*2/*c*	*C*2/*c*
a	13.3611(4) Å	13.3612(15) Å	13.3612(15) Å
b	6.4923(2) Å	6.4977(7) Å	6.4977(7) Å
c	10.0611(3) Å	10.0383(12) Å	10.0383(12) Å
β	119.818(1)°	119.854(5)°	119.854(5)°
V	757.20(4) Å^3	755.85(15) Å^3	755.85(15) Å^3
Z	8	8	8
empirical formula	$(Mn_{1.701}Mg_{0.153}Fe^{3+}_{0.054}Fe^{2+}_{0.051}Ca_{0.041})_{\Sigma=2}$ $(P_{0.973}Fe^{3+}_{0.027})_{\Sigma=1}$ O_4 $(OH_{0.666}F_{0.334})_{\Sigma=1}$		
refined chemistry	$(Mn_{0.95}Ca_{0.05})(Mn_{.75}Fe_{0.10}Mg_{0.15})(PO_4)(OH_{0.67}F_{0.33})$		
calc. density	3.835 g/cm^3	3.819 g/cm^3	3.819 g/cm^3
T	293 K	100K	100 K
crystal size	160 × 120 × 50 µm	140 × 110 × 30 µm	140 × 110 × 30 µm
max 2θ	71°	103°	103°
total refl.	1595	3645	3645
obs. (F > 4σ)	1433	3438	3438
index range	–21 = h = 20 –10 = k = 10 –14 = l = 16	–26 = h = 29 –12 = k = 12 –21 = l = 19	–26 = h = 29 –12 = k = 12 –21 = l = 19
R_{sym}	3.03%	2.19%	2.19%
R_{obs}	2.27%	1.74%	1.70%
R_{all}	2.59%	1.93%	1.88%
GooF (overall)	1.048	1.102	1.126

Table 5. Atomic coordinates and atomic displacement parameters for triploidite at 293 K.

	x	y	z	U_{iso}	U_{11}	U_{22}	U_{33}	U_{12}	U_{13}	U_{23}
M1	0.05577(2)	0.26604(4)	0.99520(3)	0.01105(7)	0.0107(1)	0.0135(1)	0.0095(1)	0.0027(1)	0.0054(1)	0.0019(1)
M2	0.34364(2)	0.39547(4)	0.64742(3)	0.00874(7)	0.0111(1)	0.0075(1)	0.0089(1)	-0.0005(1)	0.0059(1)	0.0002(1)
P	0.17600(3)	0.40650(5)	0.80583(4)	0.00672(8)	0.0071(2)	0.0065(1)	0.0058(2)	0.0000(1)	0.0026(1)	0.0001(1)
O1	0.3065(1)	0.0820(2)	0.5820(1)	0.0114(2)	0.0152(5)	0.0091(4)	0.0091(5)	-0.0004(3)	0.0055(4)	0.0022(3)
O2	0.2097(1)	0.1425(2)	0.1893(1)	0.0121(2)	0.0091(5)	0.0169(5)	0.0113(5)	0.0033(4)	0.0059(4)	0.0018(4)
O3	0.4158(1)	0.0355(2)	0.3580(1)	0.0125(2)	0.0117(5)	0.0139(5)	0.0075(4)	-0.0008(4)	0.0014(4)	0.0021(4)
O4	0.3670(1)	0.2834(2)	0.1448(1)	0.0116(2)	0.0131(5)	0.0093(4)	0.0129(5)	-0.0021(4)	0.0068(4)	0.0009(4)
F	0.0159(1)	0.0968(2)	0.3927(1)	0.0217(2)	0.0182(5)	0.0230(5)	0.0285(6)	-0.0032(4)	0.0150(5)	-0.0106(4)

Table 6. Atomic coordinates and atomic displacement parameters for triploidite at 100 K. In this data set, all of the OH^- and F^- in the structure were fitted into a single site. This solution has a slightly higher R value (see table 4) than the model listed in Table 7.

	x	y	z	U_{iso}	U_{11}	U_{22}	U_{33}	U_{12}	U_{13}	U_{23}
M1	0.055676(7)	0.265715(14)	0.995320(10)	0.00551(2)	0.00499(3)	0.00657(3)	0.00503(3)	0.00120(2)	0.00255(2)	0.00091(2)
M2	0.343902(8)	0.395632(14)	0.647678(10)	0.00419(2)	0.00519(3)	0.00339(3)	0.00436(3)	-0.00014(2)	0.00265(2)	0.00015(2)
P	0.17596(1)	0.40677(2)	0.80602(2)	0.00368(2)	0.00352(4)	0.00351(5)	0.00333(5)	0.00009(3)	0.00120(4)	0.00005(3)
O1	0.30620(4)	0.08238(7)	0.58155(5)	0.00662(6)	0.0089(1)	0.0048(1)	0.0058(1)	-0.0003(1)	0.0034(1)	0.0013(1)
O2	0.20975(4)	0.14273(7)	0.18922(5)	0.00674(6)	0.0050(1)	0.0089(2)	0.0067(1)	0.0017(1)	0.0032(1)	0.0008(1)
O3	0.41626(4)	0.03503(7)	0.35807(5)	0.00699(6)	0.0061(1)	0.0077(2)	0.0044(1)	0.0001(1)	0.0005(1)	0.0012(1)
O4	0.36719(4)	0.28304(7)	0.14446(5)	0.00657(6)	0.0071(1)	0.0048(1)	0.0076(2)	-0.0011(1)	0.0035(1)	0.0008(1)
F	0.01546(4)	0.09575(8)	0.39271(7)	0.01394(8)	0.0111(2)	0.0140(2)	0.0203(2)	-0.0032(1)	0.0105(2)	-0.0085(1)

Table 7. Atomic coordinates and atomic displacement parameters for triploidite at 100 K. The order-disorder of the F site of Table 6 was resolved into a split sites, F1 and F2. The splitting of sites reduced the final R value by 0.05%.

	x	y	z	U_{iso}	U_{11}	U_{22}	U_{33}	U_{12}	U_{13}	U_{23}
M1	0.05568(1)	0.26571(1)	0.99532(1)	0.00551(2)	0.00499(3)	0.00658(3)	0.00503(3)	0.00120(2)	0.00255(2)	0.00091(2)
M2	0.34390(1)	0.39563(1)	0.64768(1)	0.00419(2)	0.00518(3)	0.00340(3)	0.00436(3)	-0.00014(2)	0.00265(2)	0.00015(2)
P	0.17596(1)	0.40676(2)	0.80602(2)	0.00368(2)	0.00352(4)	0.00350(5)	0.00334(5)	0.00009(3)	0.00120(3)	0.00005(3)
O1	0.30620(4)	0.08237(7)	0.58154(5)	0.00663(5)	0.0089(1)	0.0048(1)	0.0058(1)	-0.0003(1)	0.0034(1)	0.0013(1)
O2	0.20974(3)	0.14273(7)	0.18921(5)	0.00675(5)	0.0050(1)	0.0089(2)	0.0068(1)	0.0017(1)	0.0033(1)	0.0008(1)
O3	0.41626(3)	0.03502(7)	0.35807(5)	0.00699(6)	0.0061(1)	0.0077(1)	0.0045(1)	0.0001(1)	0.0005(1)	0.0012(1)
O4	0.36719(4)	0.28304(7)	0.14445(5)	0.00658(5)	0.0071(1)	0.0048(1)	0.0076(2)	-0.0011(1)	0.0035(1)	0.0008(1)
F1 $OH_{0.67}$	0.0136(4)	0.0996(6)	0.3892(5)	0.0140(5)	0.0078(4)	0.0170(12)	0.0194(8)	-0.0036(7)	0.0084(5)	-0.0112(7)
F2 $F_{0.33}$	0.0194(9)	0.0899(13)	0.3992(11)	0.0117(9)	0.015(2)	0.006(1)	0.018(1)	0.000(1)	0.011(1)	-0.000(1)

APPENDIX C

Sb_CLAUDETITE, $AsSbO_3$, A NEW MINERAL FROM TSUMEB, NAMIBIA.

Marcus J. Origlieri[1*]

Robert T. Downs[1§]

David W. Bunk[2]

William W. Pinch[3]

[1]Department of Geosciences, University of Arizona, Tucson, Arizona 85721–0077 USA

[2]1441 West 46th Avenue, Unit 8, Denver, CO 80211 USA;

dave@davebunkminerals.com

[3]19 Stonebridge Lane, Pittsford, NY 14534 USA; wwpinch@hotmail.com

*marcus@mineralzone.com; §downs@geo.arizona.edu

Abstract

Sb_claudetite is a new mineral with ideal chemistry $AsSbO_3$, found with leiteite, ludlockite, and quartz in a vug in massive tennantite from the Tsumeb mine, Namibia. The symmetry is monoclinic, $P2_1/n$, with a = 4.5757(4) Å, b = 13.1288(13) Å, c = 5.4216(5) Å, β = 95.039(4)°, V = 324.44(5) $Å^3$, Z = 4, and d_{calc} = 5.009 g/cm^3. Sb_claudetite forms adamantine, colorless bladed crystals to 6 mm, bound by {010}, {110}, {111}, and {$\bar{1}$01}. The mineral is flexible with perfect cleavage on {010}. Sb_claudetite is isostructural with claudetite. The crystal structure consists of corrugated sheets of corner-sharing AsO_3 and SbO_3 trigonal pyramids arranged in an ordered, alternating pattern. Raman spectra of Sb_claudetite, claudetite, and leiteite are presented and compared.

Introduction

One of the authors (DWB) obtained an unusual Tsumeb specimen containing a well- formed leiteite ($ZnAs_2O_4$) blade, red fibrous ludlockite, smithsonite, and an undetermined mineral in separate colorless crystals to 6 mm. In situ, non-destructive examination of the unknown mineral with Raman spectroscopy failed to match a pattern from a large Raman spectral database that our laboratory is currently constructing. Raman spectroscopy confirmed the identity of the separate unknown crystals with each other. Similarities to the Raman spectrum of leiteite indicated an arsenite structure and preliminary electron dispersive spectroscopy indicated As and Sb (and no other elements with $Z < 9$). Assuming an oxide composition for the phase, and since no existing mineral contains only As, Sb, and O, the authors initiated a full characterization of this mineral.

Crystal structure determination (Origlieri et al. 2006) and electron microprobe analysis identify this phase as the natural equivalent of $AsSbO_3$ (Bodenstein et al. 1983), which is isostructural with claudetite (As_2O_3) (Pertlik, 1978). The crystal structure consists of corrugated sheets of corner sharing AsO_3 and SbO_3 trigonal pyramids, with sheets stacked along [010]. The mineral and mineral name have !!NOT YET!! received approval from the Commission on New Minerals and Mineral Names of the International Mineralogical Association. The name Sb_claudetite alludes to the presence of antimony and the structural relationship with claudetite.

Strunz et al. (1958) first reported claudetite from Tsumeb as gypsum-like platelets. Strunz (1959) further elaborated, describing 1–3 mm colorless to white crystals

with unit cell dimensions a = 5.3 Å, b = 13.0 Å, c = 4.56 Å, and β ~ 94º. He sublimated the mineral and condensed minute octahedral crystals. This microchemical behavior is consistent with known behavior of claudetite, which condenses in octahedra (i.e. arsenolite). However, these tests are not sufficient to distinguish claudetite from Sb_claudetite. $AsSbO_3$ also has a cubic modification with the same crystal structure as As_2O_3 (arsenolite) (Hayek et al. 1963). Consequently, sublimation of either claudetite or Sb_claudetite would produce octahedral crystals. The unit cell reported by Strunz (1959) lacks the precision required to distinguish Sb_claudetite from claudetite. Keller et al. (1979) reported another occurrence of claudetite from Tsumeb in association with warikhanite, unfortunately without specifying their identification methods. These claudetite specimens require confirmation. The original identification of claudetite from Tsumeb could be in error, and specimens so labeled warrant re-examination.

Hayek et al. (1963) shows that cubic As_2O_3 (arsenolite) and cubic Sb_2O_3 (senarmontite) are miscible. Consequently, ordinary solid solution between arsenolite and senarmontite could yield cubic $AsSbO_3$, but this would not qualify as a new mineral. The ordering of Sb into a single As position of the claudetite structure is apparently unique to Sb_claudetite (Origlieri et al. 2006). A search of the literature failed to find any reports of monoclinic Sb_2O_3, however the orthorhombic form valentinite is known.

Occurrence and Paragenesis

The new mineral occurs in a vug in massive tennantite ore sample ($7 \times 5 \times 4$ cm) from the famous polymetallic deposit at Tsumeb, Namibia. The largest opening of 3 cm across hosts quartz crystals to 3 mm, a single terminated leiteite blade 20 by 7 mm, red fibers of ludlockite, and separate crystals of the new mineral to 6 mm. Figure 1 shows a photomicrograph of the largest group of Sb_claudetite crystals. Although we do not know the specific origin of the specimen within the Tsumeb mine, the association with leiteite leads to certain conclusions. Leiteite occurs in the second and third oxidation zones at the Tsumeb mine (Gebhard 1991, 1999). Type leiteite occurred with tennantite, chalcocite, smithsonite, and schneiderhöhnite (Cesbron et al. 1977). Our present leiteite sample occurs on tennantite matrix with quartz and ludlockite, and smithsonite. Its specific origin within the Tsumeb mine could be distinct from other known leiteite occurrences.

Although antimony minerals are not typical of the arsenic rich assemblages at Tsumeb, primary tennantite contains substantial antimony (Moritz, 1933). Antimony dominant phases include famatinite, stibnite, stibiconite, and nadorite (Schneider, 1992). Schneider (1992) lists the 1988 production of $NaSb(OH)_6$ at the Tsumeb smelter as 156 metric tons. Oxidation of host tennantite could readily supply both the arsenic and antimony required for Sb_claudetite. Moritz (1933) further notes a substantial zinc content in Tsumeb tennantite, which could supply both the zinc and arsenic requires to form leiteite ($ZnAs_2O_4$).

Monoclinic As_2O_3 forms above 250º C while cubic As_2O_3 has a melting point near 275º C (Schulman and Schumb, 1943). Hayek et al. (1963) note a melting point of 315º C for claudetite. Therefore the claudetite structure has a higher temperature stability field than that of arsenolite. Bodenstein et al. (1983) synthesized their monoclinic $AsSbO_3$ at about 347º C. Consequently, monoclinic $AsSbO_3$ would form at higher temperatures than the cubic phase. This information allows us to bracket the formation of this mineral assemblage between 275º C and 375º C in the Tsumeb deposit.

Appearance and Physical Properties

Sb_claudetite forms bladed crystals to 6 mm bound by forms {010}, {110}, {111}, and {$\bar{1}$01}. These crystals mimic the habit of claudetite from Imperial Valley, California as illustrated by Palache (1934), shown in Figure 2. Sb_claudetite is colorless and transparent with an adamantine luster. Hardness is ~2. The mineral has perfect cleavage on {010}, readily obtained. Cleavage plates are flexible, and deform similarly to gypsum.

X-ray diffraction

We used a Bruker X8 Apex diffractometer equipped with a 4K Apex II CCD detector served to generate X-ray diffraction patterns with monochromatic MoKα radiation generated at 50 kV and 35 mA. A cleavage fragment of $220 \times 70 \times 30$ µm produced diffraction spots with streaking along constant 2θ. Despite the poor appearance of the data, the reflections yielded a merged R_{int} value of 3.08%. A data collection strategy collected 1863 frames in 6 scans, from which the Bruker software generated the empirical powder pattern summarized in Table 2 and plotted in Fig. 3. We used Bruker Saint 7.16b to fit the unit cell parameters from the positions of 6609 reflections to 82º 2θ, and Bruker Shelxtl 6.14 to determine the space group. Table 3 presents the unit cell for the new mineral.

We compare the unit cell dimensions of Sb_claudetite and claudetite (Origlieri et al. 2006) in Table 3. The unit cell data of Tsumeb claudetite reported by Strunz (1959) unfortunately lacks the precision to distinguish claudetite from Sb_claudetite.

Chemistry

A cleavage plate of the unknown mineral attached to a glass disc served as the microprobe sample. Qualitative WDS scans showed only As and Sb and no other elements with Z > 9. Standardized analysis employed a Cameca SX-50 in quantitative WDS mode. Operating conditions were 15 kV and 30 nA with a beam diameter of 1.5 μm. Enargite (As) and stibiotantalite (Sb) served as standards. Data reduction and correction followed the PAP method (Pouchou & Pichoir 1984, 1985).

Table 1 lists the results of ten separate microprobe spot analyses. The average of these analyses with standard deviations is: 55.77(1.07)% Sb_2O_3 and 45.15(0.95)% As_2O_3. Normalized to three oxygen atoms, the average composition is $As_{1.088}Sb_{0.912}O_3$. The composition remained constant over the sampled regions. In the solution of the crystal structure, the idealized formula $AsSbO_3$ yielded a smaller error than the microprobe formula (Origlieri et al. 2006). For the purposes of this study, we use the fully ordered composition $AsSbO_3$ with the impression that it more accurately represents the chemistry of Sb_claudetite.

Raman Spectroscopy

Raman spectroscopy provides a nondestructive and rapid means to distinguish claudetite from the new mineral. Samples compared include the Sb_claudetite fragment from X-ray study; claudetite from Jachymov, Czech Republic (RRUFF R050133); and leiteite from Tsumeb, Namibia (RRUFF R040011). We obtained Raman spectra with a benchtop 100 mW Ar-ion laser centered at 514.532 nm and a Jobin Yvon Spex HR 460 spectometer equipped with a liquid nitrogen cooled Princeton Instruments 1152 × 256 pixel CCD detector. Using a 1200 groves mm^{-1} grating centered at 530.4 nm and Roper Instruments Winspec/32 software, we collected the shifted region from 113 to 1016 cm^{-1}.

Figure 2 compares the Raman spectra of the Sb_claudetite, claudetite, and leiteite, all in unknown orientations. The spectrum of the Sb_claudetite shows 22 vibrational modes. Raman selection rules for the claudetite and Sb_claudetite structures allow for 15 A_g modes and 15 B_g modes, not all of which may be visible. Table 5 lists the principal Raman peak positions for Sb_claudetite, claudetite, and leiteite. Additionally, Raman spectroscopy in the region between 3000–4000 rel cm^{-1} showed no active Raman modes of greater significance than background, demonstrating that the mineral is nominally anhydrous.

Acknowledgements

We graciously acknowledge the support of Michael Scott for supporting the creation of a Raman database of all known mineral species.

References

Bodenstein, D., A. Brehm, P.G. Jones, E. Schwarzmann, and G.M. Sheldrick (1983) Darstellung und Kristallstruktur von monoklinem Arsen(III)antimon(III)oxid, $AsSbO_3$. Zeitschrift für Naturforschung, Teil B, 38B, 901–904.

Cesbron, F.P., R.C. Erd, G.K. Czamanski, and H. Vachey (1977) Leiteite, a new mineral from Tsumeb. Mineralogical Record, 8(3), Tsumeb issue, 95–97.

Gebhard, G. (1991) Tsumeb: eine deutsch-afrikanische Geschichte. Verlag Christel Gebhard, Giesen, Germany. 239 pp.

Gebhard, G. (1999) Tsumeb II. CG Publishing, Waldbrol, Germany. 328 pp.

Hayek, E., P. Inama, and B. Schatz (1963) Mischkristallbildung von As_2O_3 und Sb_2O_3. Monatshefte für Chemie, 94, 366-372.

Keller, P., H. Hess, and P.J. Dunn (1979) Warikhanit, $Zn_3[(H_2O)_2|(AsO_4)_2]$, ein neues Mineral aus Tsumeb, Südwestafrika. Neues Jahrbuch für Mineralogie Monatshefte, 389-395.

Moritz, H. (1933) Die sulfidischen Erze der Tsumeb-Mine von Ausgehenden bis zur XVI. Sohle (-460 m). Neues Jahrbuch für Mineralogie, Geologie, und Paläontologie, 67A, 118-154, Tafeln XIII-XIV.

Palache, C. (1934) Contributions to crystallography: claudetite, minasragrite, samsonite, native selenium, indium. American Mineralogist, 19, 194–205.

Pertlik, F. (1978) Verfeinerung der Kristallstruktur des Minerals Claudetit, As_2O_3 ("Claudetit I"). Monatshefte für Chemie, 109, 277–282.

Pouchou, J.L. and Pichoir, F. (1984) Un nouveau modèle de calcul pour la microanalyse quantitative par spectrométrie de rayons X. Partie I: Application a l'analyse d'énchantillons homogènes. La Recherche Aérospatiale, number 3, 167–192.

Pouchou, J.L. and F. Pichoir (1985) "PAP" $\phi(\rho Z)$ procedure for improved quantitative microanalysis. In Armstrong, J.T. ed. (1985) Microbeam Analysis 1985, San Francisco Press, 104–106.

Schneider, G.I.C. (1992) Antimony. In The Mineral Resources of Namibia. First Edition. Namibia Geological Survey.

Schulman, J.H. and Schumb, W.C. (1943) The polymorphism of arsenious oxide. Journal of the American Chemical Society, 65, 878-883.

Strunz, H. (1959) Tsumeb, seine Erze und Sekundärmineralien, insbesondere der neu aufgeschlossenen zweiten Oxydationszone. Forschritte der Mineralogie, 37, 87–90.

Strunz, H., G. Söhnge and B.H. Geier (1958) Stottit, ein neues Germanium-Mineral und seine Paragenese in Tsumeb. Neues Jahrbuch für Mineralogie Monatshefte, 85–96.

Table 1. Microprobe analyses for the new mineral, and their corresponding atomic compositions normalized to three oxygen atoms. The average of these analyses, with standard deviations is 55.77(1.07)% Sb_2O_3 and 45.15(0.95)% As_2O_3. Normalized to three oxygen atoms, the average composition is $As_{1.088}Sb_{0.912}O_3$.

% Sb_2O_3	% As_2O_3	total	composition
55.03	45.66	100.69	$As_{1.100}Sb_{0.900}O_3$
55.46	44.57	100.02	$As_{1.084}Sb_{0.916}O_3$
56.39	44.82	101.22	$As_{1.079}Sb_{0.921}O_3$
55.64	43.95	99.59	$As_{1.076}Sb_{0.924}O_3$
56.13	44.30	100.43	$As_{1.075}Sb_{0.925}O_3$
56.33	46.62	102.95	$As_{1.099}Sb_{0.901}O_3$
56.77	44.54	101.31	$As_{1.072}Sb_{0.928}O_3$
56.76	46.75	103.51	$As_{1.097}Sb_{0.903}O_3$
53.16	45.50	98.67	$As_{1.116}Sb_{0.884}O_3$
56.05	44.74	100.80	$As_{1.081}Sb_{0.919}O_3$

Table 2. Powder diffraction data for the new mineral plotted in Fig. 3.

d	I/I_0	h	k	l
4.9946	31.87	0	1	1
3.6446	11.42	-1	0	1
3.5118	100	-1	1	1
3.4001	18.29	0	3	1
3.3416	14.28	1	0	1
3.2822	82.13	0	4	0
3.2384	71.21	1	1	1
3.1568	23.86	1	3	0
2.8048	38.8	0	4	1
2.8006	30.75	-1	3	1
2.7003	23.41	0	0	2
2.6559	28.08	1	3	1
2.645	23.98	0	1	2
2.279	34.29	2	0	0
2.2692	8.24	-1	2	2
2.2454	5.15	2	1	0
2.1401	5.27	-2	1	1
2.1304	9.28	-1	5	1
2.1188	7.83	1	2	2
2.0853	16.89	0	4	2
2.0646	12.89	1	5	1
1.8825	10.03	0	5	2
1.872	20.65	2	4	0
1.8223	8.01	-2	0	2
1.8096	6.37	-2	4	1
1.805	5.42	-2	1	2
1.7344	16.19	1	7	0
1.7305	6.69	2	4	1
1.727	5.13	-1	0	3
1.6649	6.64	0	3	3
1.6574	6.19	2	1	2
1.6263	6.83	1	0	3
1.6064	6.01	-1	3	3
1.5932	6.32	-2	4	2
1.5702	16.8	0	8	1
1.4876	7.25	-3	1	1
1.4572	7.43	1	4	3
1.3087	7.28	-2	8	1

Table 3. Comparison of the unit cells of claudetite and Sb_claudetite. Claudetite data are from Origlieri et al. (2006).

	Sb_claudetite	claudetite
idealized formula	$AsSbO_3$	As_2O_3
space group	$P2_1/n$	$P2_1/n$
a	4.5757(4) Å	4.5460(4) Å
b	13.1288(13) Å	13.0012(14) Å
c	5.4216(5) Å	5.3420(5) Å
β	95.039(4)°	94.329(2)°
V	324.44(5) $Å^3$	314.83(5) $Å^3$
Z	4	4
calculated density	5.009 g/cm^3	4.174 g/cm^3

Table 4. Principal Raman peak positions (shifted cm^{-1}) of the Sb_claudetite, claudetite, and leiteite in unknown orientations. Their patterns are plotted at Fig. 4.

Sb_claudetite	claudetite	leiteite
115		
125		125
		138
155		150
		168
171	175	179
183		
	193	201
202		205
210	218	220
	248	256
232	259	269
273	284	
298		307
	354	368
323	356	379
342		
414		
430		
468	459	459
477		
517		
	541	550
		603
620	626	649
631	632	
726		
766		764
817	814	806

Fig. 1. The largest cluster of crystals of the new mineral, 6 mm across, in a vug of massive tennantite with quartz crystals. D.W. Bunk specimen, now in the W.W. Pinch collection.

Fig. 2. Crystal drawing of Sb_claudetite, showing forms {010}, {110}, {111}, and {$\bar{1}$01}.

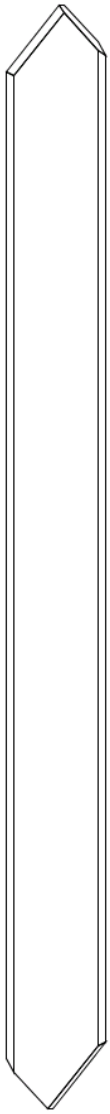

Fig 3. X-ray powder diffraction pattern for natural $AsSbO_3$. Peak positions are listed in Table 2.

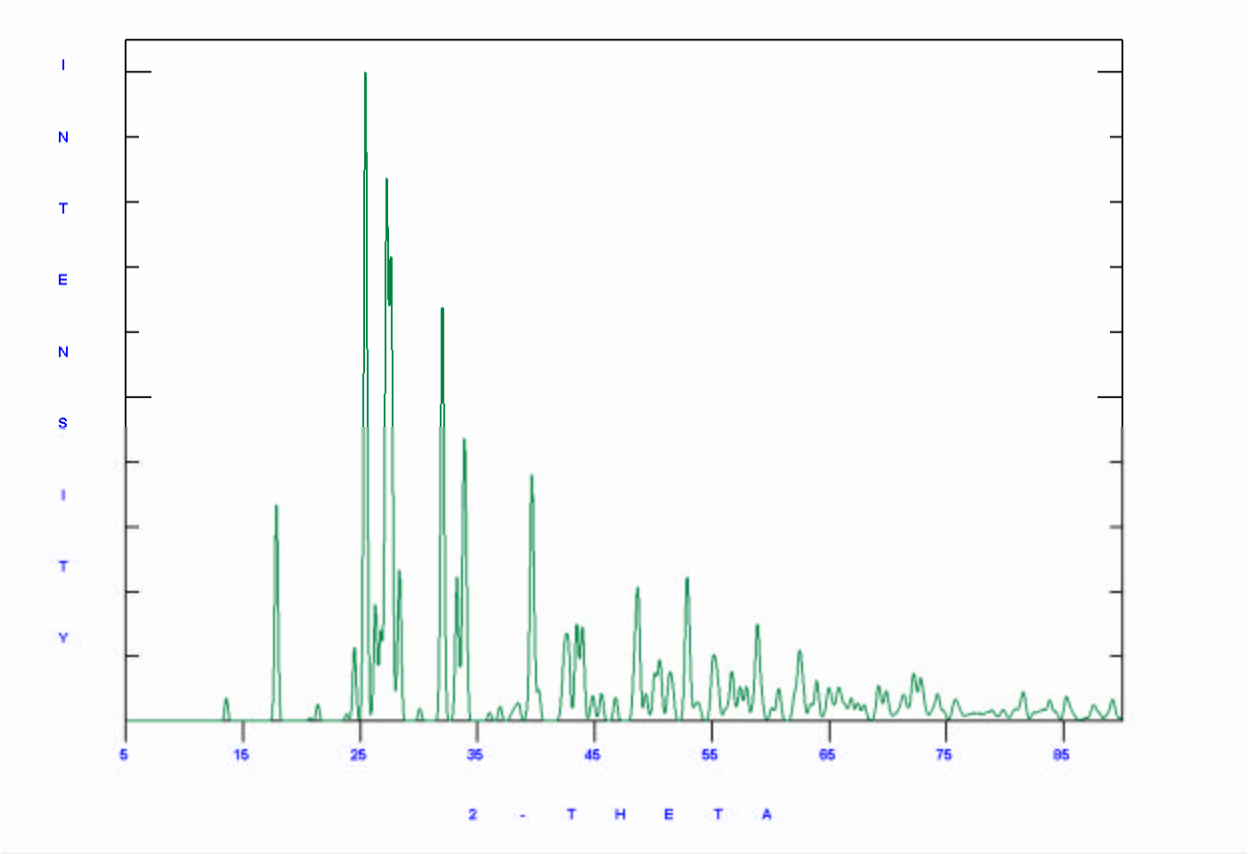

Fig. 4. Comparison of Raman spectra of Sb_claudetite, claudetite, and leiteite, all in undetermined orientations. Peak positions for both spectra are listed in Table 5.

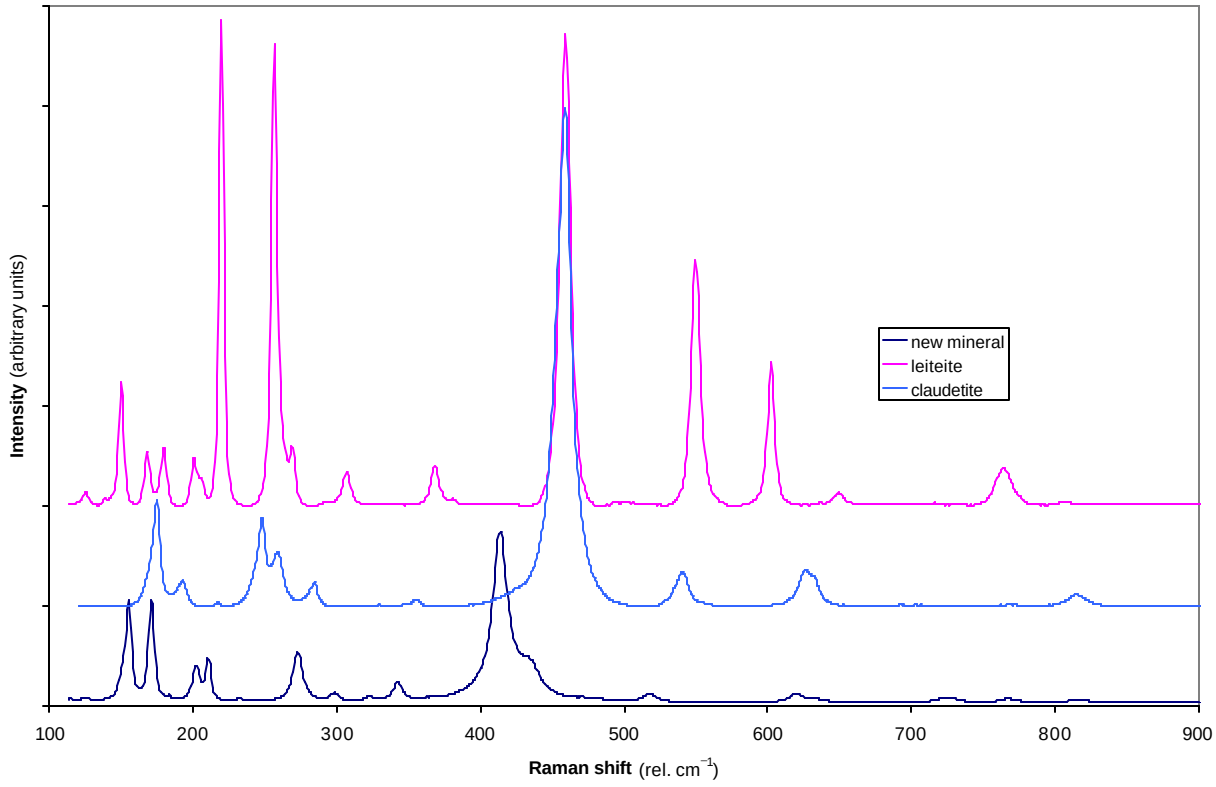

APPENDIX D

CRYSTAL STRUCTURES OF SB_CLAUDETITE, $AsSbO_3$, AND CLAUDETITE, As_2O_3, WITH ANALYSIS OF BONDING TOPOLOGIES.

Marcus J. Origlieri[1*]

Robert T. Downs[1§]

Michael D. Carducci[1]

Kevin M. Rosso[2]

G. V. Gibbs[3]

[1]Department of Geosciences, University of Arizona, Tucson, Arizona 85719–0077 USA

[2]Pacific Northwest National Laboratory, P.O. Box 999, K8-96, Richland, WA 99352 USA

[3]Department of Geological Sciences, Virginia Polytechnic Institute, Blacksburg, VA 24061–0420 USA

*marcus@geo.arizona.edu; §downs@geo.arizona.edu

Abstract

The crystal structure of the newly described mineral Sb_claudetite, $AsSbO_3$, is presented and compared with a new crystal structure refinement of the isostructural mineral claudetite, As_2O_3. Sb_claudetite has monoclinic symmetry, $P2_1/n$, with a = 4.5757(4) Å, b = 13.1288(13) Å, c = 5.4216(5) Å, β = 95.039(4)°, and V = 324.44(5) $Å^3$ with Z = 4. The crystal structure consists of corrugated sheets of corner-sharing AsO_3 and SbO_3 trigonal pyramids with average <As–O> and <Sb–O> bond lengths 1.782 Å and 1.993 Å, respectively. Electron density distributions from *ab initio* quantum calculations show several long range interactions between As and O and Sb and O in Sb_claudetite. The bonds are ranked into three separate groups by the electron density at the bond critical points. The strongest of these bonds are associated with close contacts between As and Sb with O. A distinctly weaker group of bonds stabilize the corrugation of the structural sheets. A yet distinctly weaker pair of bonds holds the sheets together and is associated with the observed cleavage plane (010). Claudetite has monoclinic symmetry, $P2_1/n$, with a = 4.5460(4) Å, b = 13.0012(14) Å, c = 5.3420(5) Å, β = 95.329(2)°, and V = 314.83(5) $Å^3$ with Z = 4. The crystal structure consists of corrugated sheets of corner linked AsO_3 trigonal pyramids, with two unique As sites.

Introduction

Origlieri et al. (2006) described Sb_claudetite as a new arsenite mineral from the Tsumeb mine, Namibia, of composition $AsSbO_3$. Electron microprobe study and single crystal X-ray diffraction methods identified Sb_claudetite (Origlieri et al. 2006) as the natural equivalent of synthetic $AsSbO_3$ (Bodenstein et al. 1983), whose crystal structure consists of corrugated sheets of corner sharing AsO_3 and SbO_3 trigonal pyramids, stacked along [010].

The Tsumeb mine has produced many new arsenite minerals including reinerite (Ghose et al. 1977), schneiderhöhnite (Hawthorne, 1985), ludlockite (Cooper and Hawthorne, 1996) and leiteite (Ghose et al. 1987), which all share similar AsO_3 groups, variously as isolated AsO_3 groups, As_2O_5 dimers, As_5O_{11} segments, and infinite As_2O_4 chains. Further polymerization of AsO_3 groups by sharing all three oxygen atoms results in the formula As_2O_3, which occurs as isolated As_4O_6 units in arsenolite (Ballirano and Maras, 2002) and infinite sheets of As_2O_3 in claudetite (Pertlik, 1978).

Crystal structures containing AsO_3 and SbO_3 units have received attention since the dawn of X-ray diffraction. Arsenolite (cubic As_2O_3) and senarmontite (cubic Sb_2O_3) were solved by Bozorth (1923), and shown to consist of four fully polymerized MO_3 groups arranged in an M_4O_6 octahedron. Valentinite, the orthorhombic phase of Sb_2O_3, was solved by Buerger (1936) and Bloom and Buerger (1937), and consists of fully corner linked SbO_3 groups, resulting in infinite double chains of composition Sb_2O_3. Claudetite, the monoclinic form of As_2O_3, was solved by Frueh (1951), and shown to

consist of infinite sheets of fully corner linked AsO_3 groups, resulting in a composition As_2O_3.

Long range interactions between As and O have been examined in the structures of trippkeite (Pertlik, 1975) and leiteite (Ghose et al. 1987). Pertlik (1975) studied trippkeite ($CuAs_2O_4$) and disregarded the bonding potential of long range As–O interactions (3.15 Å) as repulsive steric effects.

Ghose et al. (1987) solved the structure of leiteite, $ZnAs_2O_4$, and found it to consist of sheets of ZnO_4 tetrahedra held together with chains of AsO_3. Ghose et al. (1987) proposed a long range As-O bonding scheme to hold the sheets together, responsible for much of its soft lamellar cleavage. However, these studies suffered from the lack of quantitative approach, which would require a definition of bonded interactions.

Recently, Bader (1990) and his colleagues have proposed a strategy for analyzing the topology of molecules and crystals in terms of the distribution of critical points in the electron density. These are points with a zero value for the gradient of the electron density. These points include (1) maxima, which correspond to positions of atoms, (2) minima, and (3) saddle points. In particular, Bader (1998) describes a pair of atoms as bonded if and only if there exists a bond path and a saddle point in the electron density between that pair of atoms. A bond path is a line, not necessarily straight, of continuous local maxima in the perpendicular plane which connect the atoms. The saddle point, referred to as a bond critical point (bcp), is the point of local minimum along the bond

path. The determination of the location of bcp's in a crystal provides coordination numbers for the various atoms in the structure, as well as a topological classification. Associated with each bcp is (1) the value of the electron density at that point, ? , related to the bond strength (Gibbs et al. 2001) and (2) the value of the Laplacian (?2?), related to the bond character (Bader 1990).

Whitten et al. (2004) studied the electron density distributions in two polymorphs of Sb_2O_3, valentinite and senarmontite. In valentinite, Whitten et al. (2004) noted two types of long range interactions, the first between chains, and the other were weak Sb−Sb interactions. In order to determine if any intermetallic bonding was occurring in the oxide phases Sb_claudetite and cla udetite, we ran ab initio quantum calculations to generate electron density distributions for the observed crystal structures.

Experimental

A Bruker X8 Apex diffractometer equipped with a 4K Apex II CCD detector served to study the X-ray diffraction patterns using monochromatic MoKα radiation generated at 50 kV and 35 mA. A cleavage fragment from the Tsumeb deposit, Namibia, yielded diffraction spots with streaking along constant 2θ. The data collection include 2073 unique reflections to 82º 2θ, with 1880 reflections qualifying as observed with $F_0 > 4\sigma(F_0)$. Indices spanned the ranges: $-7 \le h \le 8$, $-20 \le k \le 23$, $-10 \le l \le 7$. Despite the poor appearance of the data, the reflections yielded a merged R_{int} value of 3.08%. We obtained a cleavage fragment of claudetite from Jáchymov, Erzgebirge, Czech Republic from University of Arizona Mineral Museum catalogue number 16128. The data collection include 962 unique reflections to 61º 2θ, with 783 reflections qualifying as observed with $F_0 > 4\sigma(F_0)$. Indices spanned the ranges: $-6 \le h \le 3$, $-18 \le k \le 14$, $-7 \le l \le 7$. For both structures, absorption corrections and scaling followed an empirical multiscan method offered by the Bruker Apex2 software package. The initial structure solutions for Sb_claudetite and claudetite used direct methods (Sheldrick, 1990). Subsequent refinement cycles employed Shelx97 (Sheldrick 1997). XTALDRAW software rendered the crystal structure for viewing and generation of figures. METRIC97 software allowed confirmation of bond lengths and angles.

Procrystal software uses linear combinations of spherically averaged wave functions to create a model of the electron density distributions in crystals. These rapid

calculations provide a utilitarian screening method to obtain a meaningful bonding topology for a crystal structure. Procrystal modelling has been shown to reproduce ab initio quantum calculations within error (Downs et al. 2002). We used the Speeden (Downs et al. 1996) software to generate a bonding topology, which indicated extended metal - oxygen interactions, and consequently we initiated robust quantum calculations.

The Crystal98 program (Pisani, 1996, Pisani et al. 2000, Saunders et al. 1998) was used to generate a self-consistent analytical electron density distribution for the $AsSbO_3$. The wave function was computed at the density functional theory (DFT) level using the Kohn–Sham (1965) strategy together with the Vosko, Wilk and Nusair (1980) parameterization of the local density approximation (LDA). Crystal98 computes the wave function for crystalline systems using periodic boundary conditions and a linear combination of atomic orbitals method (LCAO). Crystalline orbitals are comprised of linear combinations of Bloch functions that are defined in terms of Gaussian-type local functions. The Gaussian-type basis sets used in molecular orbital calculations are typically too diffuse to serve as basis sets in crystal orbital calculations in that their use often results in an over-estimate of the orbital overlap and numerical instability. For this reason, we used basis sets that had been especially developed and optimized for use in Crystal98. Good convergence behavior and electron density distribution results were obtained using a DZVP (DFT orbital) basis set for Sb (Godbout et al., 1992) with diffuse functions optimized for use in antimony oxides (Whitten et al., 2004), a 9-7631G(2d) set

for As (Towler et al., 1996), and a 8-411G basis set optimized for O^{2-} (McCarthy and Harrison, 1994).

The properties of the electron density distributions were analyzed using Topond (Gatti, 1997). Bond critical point properties of the electron density distribution were computed using an automated chain-like search strategy which uses an eigenvector following method to locate critical points within a pre-defined search region. The maximum number of eigenvector following steps was set to 20, with a search radius of 9.0 Å.

Crystal Structure Determination and Refinement

Direct methods (Sheldrick, 1990) were used to locate the As and Sb atoms. Three residual peaks in the Fourier difference map at distances compatible with As–O and Sb–O bonds were assigned as oxygen atoms. At this point, the refinement converged with an R value of 8% with isotropic displacement factors. Refinement with the empirical microprobe composition gave a higher R value, despite freely varying the As and Sb contents within the two metal sites. The refinement clearly demonstrated ordering of the As and Sb atoms. The idealized formula $AsSbO_3$ was used for final structure refinement along with anisotropic displacement parameters, giving the lowest R factor of 5.66%. Poor diffraction quality is likely responsible for this rather high R value. In their solution of synthetic $AsSbO_3$, Bodenstein et al. (1983) used a point detector and employed wide omega scans due also to poor peak shape. Their data refined with a R of 5.5%, comparable to this refinement.

Table 1 lists the unit cell parameters used in the refinement. Table 2 lists the refined atomic coordinates and anisotropic displacement factors for the new mineral. The crystal structure consists of corrugated sheets of corner linked AsO_3 and SbO_3 trigonal pyramids arranged in an ordered checkerboard pattern. These sheets stack along [010] (Fig. 1). Table 4 lists refined bond lengths and selected angles.

Discussion

The structure of Sb_claudetite is essentially identical to that reported for the synthetic material (Bodenstein et al. 1983). While the R factors between the synthetic study (.055) and our present natural sample (.0566) are quite similar, our data set has nearly triple the number of observed reflections giving more precise unit cell parameters, bond lengths, and geometries. We have confirmed the claudetite structure of Pertlik (1978), but have switched the **a** and **c** cell edges to match the setting of Bodenstein et al. (1984). We improved the precision of the cell parameters, and furthermore refined anisotropic displacement parameters.

Arsenic in Sb_claudetite adopts a trigonal pyramidal configuration, consisting of a central out of plane As atom with short bonds to three oxygen atoms, <R(As–O)> = 1.782 Å. Isostructural claudetite, has a similar position for As1, with <R(As1–O)> = 1.783 Å. Tables 4 and 5 present the observed bond lengths and geometries for the AsO_3 group in Sb_claudetite, and for the $As1O_3$ group in claudetite, respectively. Two other arsenite minerals also from the Tsumeb deposit have comparable values of R(As–O): reinerite (Ghose et al. 1977) has <R(As-O)> = 1.768 and leiteite (Ghose et al. 1987) has <R(As–O)> = 1.784 Å. Additionally, cubic As_2O_3 (arsenolite) has R(As–O) = 1.786 Å (Ballirano & Maras, 2002). Our reported geometry for AsO_3 in Sb_claudetite has <<O–As–O> = 97.7° and claudetite has <<O–As1–O> = 98.1°, comparable to <O–As–O

= 98.4° in arsenolite (Ballirano & Maras, 2002), and <<O–As–O> = 95.7° in leiteite (Ghose et al. 1987) and <<O–As–O> = 97.6° in reinerite (Ghose et al. 1977).

Antimony in Sb_claudetite adopts a trigonal pyramidal configuration, consisting of a central out of plane Sb atom with short bonds to three oxygen atoms, <R(Sb–O)> = 1.993 Å. The observed bond lengths for Sb–O are listed in Table 4. They compare well with those found in SbO_3 groups in synthetic senarmontite (cubic Sb_2O_3) with R(Sb–O) = 1.978 Å found by Whitten et al. (2004) and those in synthetic valentinite (orthorhombic Sb_2O_3), for which Svensson (1974) observed <R(Sb–O)> = 2.006 Å. Our reported O–Sb–O angles display a smaller range (84.8°–93.0°) than those Svensson (1974) reported for valentinite (79.8°, 91.9°, 98.1°). Whitten et al. (2004) observed <O–Sb–O = 95.87° in senarmontite, while Svensson (1974) reports <<O–Sb–O> = 89.9° in valentinite which compares with favorably with our reported <<O–Sb–O> = 90.0°. In isostructural claudetite, the As2 corresponds to the Sb in Sb_claudetite. In claudetite, <R(As2–O)> = 1.793 Å, which is .200 Å shorter than <R(Sb–O)> in Sb_claudetite. For claudetite, <<O–As2–O> = 94.8° is significantly smaller than <<O–As1–O> = 98.1°, which is closer to the smaller angles observed for <<O–Sb–O> in Sb_claudetite. Since the average bond lengths of the two distinct As sites are essentially identical, Sb likely orders into the As2 site due to its narrower angles. Senarmontite also displays a smaller <O–Sb–O than <O–As–O in isostructural arsenolite. Furthermore, synthetic $AsSbO_3$ (Bodenstein et al. 1983) has <R(As–O)> = 1.80 Å and <R(Sb–O)> = 1.95 Å, while

Sb_claudetite shows a shorter <R(As–O)> and a longer <R(Sb–O)>, consistent with a higher degree of As/Sb ordering in the natural phase.

In Sb_claudetite, trigonal pyramids of AsO_3 and SbO_3 link corners, such that every O in the structure is a bridging O, forming continuous sheets. These sheets show a pronounced corrugation with channels aligned parallel to [100] as illustrated in Fig. 1. Analysis of the electron density calculations show three additional bonds that stabilize the corrugation of the sheets. We call these intra-layer bonds, and list their properties in Table 4. Parallel to the channels are the two bonds, As–O2 at 2.903 Å and Sb–O3 at 2.791 Å, which stabilize the ridges of the corrugated sheet. An additional Sb–O1 bond at 2.947 Å stabilizes the open channels in the corrugated sheet. Figure 2 shows the positions of the intra-layer bonds.

In claudetite, two distinct AsO_3 trigonal pyramids also link corners to form continuous sheets. These sheets are held together by six close contact bonds. These sheets show a pronounced corrugation parallel to [100]. Analysis of the electron density distributions from quantum calculations shows an additional long range As2-O1 interaction at 3.033 Å. The bond critical point properties for this interaction are given in Table 7. This bond is perpendicular to the corrugation and essentially identical to the Sb-O1 interaction observed in the stibioclaudetite structure. Curiously, the claudetite shows a single intra-layer bond, while the Sb_claudetite shows three intra-layer bonds. The most likely explanation is the much larger electron density of Sb puts an additional 72

electrons into the unit cell volume. These electrons result in the two additional bonds in Sb_claudetite.

In Sb_claudetite and claudetite, corrugated sheets of $AsSbO_3$ and As_2O_3, respectively, stack along (010), which serves as the cleavage plane in this structure. Analysis of electron density calculations in Sb_claudetite shows two long bonds between the layers, Sb–O2 at 3.237 Å and As–O3 at 3.346 Å, which we call inter-layer bonds. Claudetite shows the corresponding interaction, As2–O2 at 3.356 Å and As1–O3 at 3.429 Å. Figure 3 illustrates the connectivity of the inter-layer bonds in Sb_claudetite, and Table 6 lists their properties.

The magnitudes of electron density and their corresponding Laplacian and eigenvalues at the critical points vary with the observed bond lengths. The strongest bonds are As–O close contacts, which are shorter than Sb–O close contacts, and have larger electron densities at their critical points ($\rho(r_c)$). The Sb–O bonds curiously have larger Laplacian values than the As–O bonds, even though the values of critical point electron density of the As–O are larger than those of Sb–O. Intra-layer bonds have a distinct population of critical point electron densities much smaller than those observed for the close contacts. The inter-layer bonds have yet distinctly smaller values of $\rho(r_c)$, nearly half those of the intra-layer bonds, which explains the separation of the layers on the observed cleavage plane.

Long range Sb–O interactions have been previously observed in senarmontite and valentinite (Whittten et al. 2004)

Long range As–O interactions may occur in other arsenites. A cursory examination of the crystal structures of reinerite and armangite, zimbabweite, magnussonite, syndelphaite, hematolite, all with isolated AsO_3 groups, show no additional O atoms within 3.5 Å of the As in AsO_3. Consequently, we do not see the possibility of the long range interactions as seen in the structures of Sb_claudetite and claudetite.

Polymerized AsO_3 and SbO_3 show influences of long range bonding. Segments of Sb_3O_7 in versilaite have Sb–O at 3.49 Å, stabilized by long range interactions. Ludlockite has numerous As–O interactions under 3.5 Å. These long range interaction appear to stabilize the structures of polymerized AsO_3 and SbO_3. Furthermore, there is a rather large number of minerals with polymerized AsO_3 minerals compared to the total number of minerals with AsO_3 groups. The tendency to polymerize likely increases due to the long range interactions of metal and oxygen in structures with AsO_3 and SbO_3.

Acknowledgements

We graciously acknowledge Michael Scott for supporting the creation of a Raman database of all known mineral species. We also thank both Michael Scott and the University of Arizona for funding sufficient to purchase the Bruker X8 diffractometer.

References

Bader, R.F.W. (1990) Atoms in molecules. Oxford Science Publications, Oxford, U.K.

Bader, R.F.W. (1998) A bond path: A universal indicator of bonded interactions. Journal of Physical Chemistry, 102A, 7314–7323.

Ballirano, P. and A. Maras (2002) Refinement of the crystal structure of arsenolite, As_2O_3. Zeitschrift für Kristallographie: New Crystal Structures, 217, 177–178.

Bodenstein, D., A. Brehm, P.G. Jones, E. Schwarzmann, and G.M. Sheldrick (1983) Darstellung und Kristallstruktur von monoklinem Arsen(III)antimon(III)oxid, $AsSbO_3$. Zeitschrift für Naturforschung, 38B, 901–904.

Bozorth, R.M. (1923) The crystal structures of the cubic forms of arsenious and antimonous oxides. Journal of the American Chemical Society, 45, 1621–1627.

Buerger, M.J. (1936) American Mineralogist 21, 206-207

Buerger, M.J. and S.B. Hendricks (1938) Zeitschrift für Kristallographie, 98, 1–30.

Cesbron, F.P., R.C. Erd, G.K. Czamanski, and H. Vachey (1977) Leiteite, a new mineral from Tsumeb. Mineralogical Record, 8, no. 3, 95–97.

Cooper, M.A. and F.C. Hawthorne (1996) The crystal structure of ludlockite, $PbFe^{3+}{}_4As^{3+}{}_{10}O_{22}$, the mineral with pentameric arsenite groups and orange hair. Canadian Mineralogist, 34, 79–89.

Downs, R.T., A. Andalman, and M. Hudacsko (1996) The coordination numbers of Na and K atoms in low albite and microcline as determined from a procrystal electron-density distribution. American Mineralogist, 81, 1344–1349.

Downs, R.T., G.V. Gibbs, M.B. Boisen Jr. and K.M. Rosso (2002) A comparison of procrystal and ab initio model representations of the electron-density distributions of minerals. Physics and Chemistry of Minerals, 29, 369–385.

Frueh, A.J. Jr (1951) The crystal structure of claudetite (monoclinic As_2O_3). American Mineralogist, 36, 833-850

Gatti, C. (1997) Topond96 user's manual. CNR-CSRSRC, University of Milan, Italy.

Ghose, S., P.K. Sen Gupta, and E.O. Schlemper (1987) Leiteite, $ZnAs_2O_4$: a novel type of tetrahedral layer structure with arsenite chains. American Mineralogist, 72, 629–632.

Ghose, S., P. Boving, W.A. LaChappelle, and C. Wan (1977) Reinerite, $Zn_3(AsO_3)_2$: an arsenite with a novel type of Zn-tetrahedral double chain. American Mineralogist, 62, 1129–1134.

Gibbs, G.V., Boisen, M.B., Jr., Beverly, L.L., and Rosso, K.M. (2001) A computational quantum chemical study of the bonded interactions in earth materials and structurally and chemically related molecules. In R.T. Cygan and J.D. Kubicki, Eds., Molecular modeling theory: Applications in the Geosciences, vol. 42, p. 345–382. Reviews in Mineralogy and Geochemistry, Mineralogical Society of America, Washington, D.C.

Godbout, N., Salahub, D. R., Andzelm, J., and Wimmer, E. (1992) Optimization of Gaussian-Type Basis-Sets For Local Spin-Density Functional Calculations.1. Boron Through Neon, Optimization Technique and Validation: Canadian Journal of Chemistry-Revue Canadienne De Chimie, v. 70, p. 560–571.

Hawthorne, F.C. (1985) Schneiderhohnite, $(Fe^{2+})(Fe^{3+})_3As_5O_{13}$, a densely packed arsenite structure. Canadian Mineralogist, 23, 675–679.

Kohn, W., and Sham, L. J. (1965) Self-consistent equations including exchange and correlation effects: Physical Review, A140, 1133–1138.

McCarthy, M.I. and N.M. Harrison (1994) Ab initio determination of the bulk properties of MgO: Phys. Rev. B, v. 49, p. 8574–8582.

Pertlik, F. (1975) Verfeinerung der Kristallstruktur von synthetischem Trippkeit, $CuAs_2O_4$. Tschermaks Mineralogische und Petrologische Mittelungen, 22, 211–217.

Pertlik, F. (1978) Verfeinerung der Kristallstruktur des Minerals Claudetit, As_2O_3 ("Claudetit I"). Monatshefte für Chemie, 109, 277–282.

Pisani, C. (1996) Quantum Mechanical Ab Initio Calculation of the Properties of Crystalline Materials. Springer Verlag, Berlin. 328 pp.

Pisani, C., Dovesi, R., Roetti, C., Causa, M., Orlando, R., Casassa, S., and Saunders, V. R., 2000, Crystal and Embed, two computational tools for the ab initio study of electronic properties of crystals. Int. J. Quantum Chem., v. 77, p. 1032–1048.

Saunders, V. R., Dovesi, R., Roetti, C., Causa, M., Harrison, N. M., Orlando, R., and Zicovich-Wilson, C. M. (1998) CRYSTAL98 User's Manual. University of Torino, Italy.

Sheldrick, G.M. (1990) Phase annealing in SHELX-90: Direct methods for larger structures. Acta Crystallographica, A46, 467–473.

Sheldrick, G.M. (1997) SHELXL-97, a program for crystal structure refinement. University of Göttingen, Göttingen, Germany.

Strunz, H. (1959) Tsumeb, seine Erze und Sekundärmineralien, insbesondere der neu aufgeschlossenen zweiten Oxydationszone. Forschritte der Mineralogie, 37, 87–90.

Svensson, C. (1974) The crystal structure of orthorhombic antimony trioxide, Sb_2O_3. Acta Crystallographica, B30, 458–461.

Towler, M.D., A. Zupan, and M. Causa (1996) Density functional theory in periodic systems using local Gaussian basis sets. Comp. Phys. Comm., 98, 181–205.

Vosko, S.H., Wilk, L., and Nusair, M. (1980) Accurate Spin-Dependent Electron Liquid Correlation Energies for Local Spin-Density Calculations - a Critical Analysis: Canadian Journal of Physics, 58, 1200–1211.

Whitten, A.E., B. Dittrich, M.A. Spackman, P. Turner and T.C. Brown (2004) Charge density analysis of two polymorphs of antimony(III) oxide. Dalton Transactions, 23–29.

Table 1. Refinement data for the Sb_claudetite and claudetite.

	Sb_claudetite	claudetite
refined chemistry	$AsSbO_3$	As_2O_3
space group	$P2_1/n$	$P2_1/n$
a	4.5757(4) Å	4.5460(4) Å
b	13.1288(13) Å	13.0012(14) Å
c	5.4216(5) Å	5.3420(5) Å
β	95.039(4)°	94.329(2)°
V	324.44(5) $Å^3$	314.83(5) $Å^3$
Z	4	4
refined formula	$AsSbO_3$	As_2O_3
calculated density	5.009 g/cm^3	4.174 g/cm^3
crystal size	$220 \times 70 \times 30$ µm	$170 \times 105 \times 35$ µm
maximum 2θ	82	61
# collected reflections	2073	962
# observed reflections (F>4σ)	1880	783
Rsym	2.71%	3.37%
Robs	5.66%	4.10%
Rall	6.04%	5.21%
GooF (all)	1.221	1.134

Table 2. Atomic coordinates and temperature factors for Sb_claudetite.

	x	y	z	U_{iso}	U_{11}	U_{22}	U_{33}	U_{12}	U_{13}	U_{23}
As	0.03388(18)	0.09589(6)	0.25603(15)	0.0111(2)	0.0111(3)	0.0114(3)	0.0107(3)	0.0002(2)	–0.0002(2)	0.0015(2)
Sb	0.00533(12)	0.35440(4)	0.32841(9)	0.0122(1)	0.0124(2)	0.0146(2)	0.0099(2)	0.0001(1)	0.0024(1)	0.0000(1)
O1	0.0668(17)	0.2106(5)	0.4289(13)	0.019(1)	0.027(3)	0.013(2)	0.016(2)	0.000(2)	0.000(2)	0.002(2)
O2	0.1500(14)	0.4051(5)	0.6663(12)	0.017(1)	0.010(2)	0.026(3)	0.013(2)	–0.002(2)	0.000(2)	0.005(2)
O3	0.1095(15)	0.1399(6)	0.9553(11)	0.017(1)	0.015(2)	0.026(3)	0.010(2)	0.000(2)	0.001(2)	0.004(2)

Table 3. Atomic coordinates and temperature factors for claudetite.

	x	y	z	U_{iso}	U_{11}	U_{22}	U_{33}	U_{12}	U_{13}	U_{23}
As1	0.04086(13)	0.10138(5)	0.25842(12)	0.0175(2)	0.0161(3)	0.0184(4)	0.0173(3)	0.0006(2)	-0.0034(2)	0.0021(2)
As2	0.00498(13)	0.35014(5)	0.35650(11)	0.0178(2)	0.0157(3)	0.0222(4)	0.0152(3)	-0.0003(2)	-0.0002(2)	0.0004(3)
O1	0.0694(12)	0.2179(4)	0.4305(9)	0.025(1)	0.032(2)	0.020(3)	0.022(2)	0.000(2)	-0.003(2)	-0.005(2)
O2	0.1573(10)	0.3980(4)	0.6559(9)	0.023(1)	0.015(2)	0.030(3)	0.023(2)	0.001(2)	-0.003(2)	-0.009(2)
O3	0.1380(10)	0.1411(4)	0.9546(9)	0.025(1)	0.016(2)	0.041(3)	0.018(2)	0.000(2)	-0.001(2)	0.004(2)

Table 4. Selected bond lengths (Å) and bond angles for Sb_claudetite.

As–O1	1.773(7)	Sb–O1	1.978(7)
As–O2	1.781(6)	Sb–O2	2.006(6)
As–O3	1.792(6)	Sb–O3	1.995(7)
<As–O>	1.782	<Sb–O>	1.993
O1–As–O2	100.8(3)°	O1–Sb–O2	92.2(3)°
O1–As–O3	101.1(3)°	O1–Sb–O3	93.0(3)°
O2–As–O3	91.1(3)°	O2–Sb–O3	84.8(3)°
As–O1–Sb	131.4(4)°		
As–O2–Sb	119.0(3)°		
As–O3–Sb	125.4(3)°		

Table 5. Selected bond lengths (Å) and bond angles for claudetite.

As1–O1	1.772(5)	As2–O1	1.783(5)
As1–O2	1.788(4)	As2–O2	1.805(5)
As1–O3	1.790(5)	As2–O3	1.790(5)
<As1–O>	1.783	<As2–O>	1.793
O1–As1–O2	100.8(2)°	O1–As2–O2	95.2(2)°
O1–As1–O3	102.1(2)°	O1–As2–O3	97.9(2)°
O2–As1–O3	91.3(2)°	O2–As2–O3	91.3(2)°
As1–O1–As2	134.8(3)°		
As1–O2–As2	125.0(3)°		
As1–O3–As2	125.7(3)°		

Table 6. Bond critical point properties for Sb_claudetite. The columns are $\rho(\mathbf{r}_c)$, electron density at the bond critical point; $\nabla^2\rho(\mathbf{r}_c)$, Laplacian of the electron density at the critical point; λ_1, λ_2, λ_3, eigenvalues of the Hessian; ε, ellipticity; **x**, **y**, **z** coordinates within the unit cell; $\mathbf{r}_b(O)$, bonded radius of oxygen; R(MO), metal oxygen distance; and atom names of bonded atoms. The first six rows correspond to close contacts listed in the geometry of Table 3. The remaining critical points, distinguished by their lower values of $\rho(\mathbf{r}_c)$ correspond to long range metal oxygen interactions.

$\rho(\mathbf{r}_c)$ $e^-/Å^3$	$\nabla^2\rho(\mathbf{r}_c)$ $e^-/Å^5$	λ_1	λ_2	λ_3	e	**x**	**y**	**z**	$\mathbf{r}_b$(O) Å	R(MO) Å	atom names
CLOSE CONTACTS											
1.012	8.260	–5.409	–5.394	19.06	0.0027	0.0493	0.1521	0.3380	0.913	1.773	As–O1
1.009	7.707	–5.490	–5.328	18.53	0.0303	0.8480	0.0958	0.2109	0.917	1.781	As–O2
0.984	7.432	–5.284	–5.124	17.84	0.0313	0.0731	0.1173	0.1105	0.921	1.792	As–O3
0.757	10.18	–3.327	–3.281	16.79	0.0140	0.0360	0.2807	0.3771	0.968	1.978	Sb–O1
0.730	9.781	–3.247	–3.109	16.14	0.0443	0.3046	0.1424	0.8947	0.979	1.995	Sb–O3
0.730	8.950	–3.203	–3.035	15.19	0.0554	0.5823	0.1201	0.0002	0.983	2.006	Sb–O2
INTRA-LAYER BONDS											
0.169	1.502	–0.429	–0.297	2.227	0.4460	0.8222	0.1390	0.8973	1.325	2.791	Sb–O3
0.115	1.273	–0.293	–0.148	1.714	0.9787	0.3563	0.0930	0.2058	1.379	2.903	As–O2
0.134	1.081	–0.341	–0.327	1.749	0.0455	0.2818	0.1779	0.6065	1.383	2.947	Sb–O1
INTER-LAYER BONDS											
0.084	0.686	–0.182	–0.169	1.036	0.0765	0.4264	0.0172	0.8218	1.515	3.237	Sb–O2
0.062	0.581	–0.132	–0.109	0.823	0.2079	0.9658	0.9716	0.1511	1.599	3.346	As–O3

Table 7. Bond critical point properties for claudetite. The columns are $\rho(\mathbf{r}_c)$, electron density at the bond critical point; $\nabla^2\rho(\mathbf{r}_c)$, Laplacian of the electron density at the critical point; l_1, l_2, l_3, eigenvalues of the Hessian; ε, ellipticity; **x**, **y**, **z** coordinates within the unit cell; $\mathbf{r}_b(O)$, bonded radius of oxygen; R(MO), metal oxygen distance; and atom names of bonded atoms. The first six rows correspond to close contacts listed in the geometry of Table 4. The remaining critical points, distinguished by their lower values of $\rho(\mathbf{r}_c)$ correspond to long range metal oxygen interactions.

$\rho(\mathbf{r}_c)$ $e^-/Å^3$	$\nabla^2\rho(\mathbf{r}_c)$ $e^-/Å^5$	l_1	l_2	l_3	e	**x**	**y**	**z**	$\mathbf{r}_b$(O) Å	R(MO) Å	atom names
		$e^-/Å^5$									
CLOSE CONTACTS											
1.008	8.469	–5.392	–5.343	19.20	0.0092	0.0539	0.1585	0.3398	0.912	1.772	As1–O1
0.985	7.758	–5.311	–5.176	18.24	0.0261	0.8553	0.1022	0.2067	0.920	1.788	As1–O2
0.985	7.561	–5.304	–5.125	17.99	0.0349	0.0913	0.1209	0.1118	0.922	1.790	As1–O3
0.986	7.908	–5.302	–5.225	18.43	0.0148	0.0354	0.2857	0.3901	0.918	1.783	As2–O1
0.976	7.775	–5.268	–5.162	18.21	0.0205	0.3280	0.1454	0.9061	0.922	1.790	As2–O3
0.953	7.173	–5.118	–4.932	17.22	0.0377	0.5822	0.1270	0.0015	0.927	1.805	As2–O2
INTRA-LAYER BOND											
0.093	0.928	-0.239	-0.224	1.390	0.0646	0.2879	0.1824	0.6244	1.455	3.033	As2-O1
INTER-LAYER BONDS											
0.051	0.504	–0.108	–0.086	0.698	0.2612	0.9494	0.9743	0.1505	1.640	3.429	As1–O3
0.053	0.547	-0.109	-0.096	0.752	0.1371	0.4235	0.0190	0.8449	1.615	3.356	As2–O2

FIGURE 1. A projection down **a** of the crystal structure of Sb_claudetite, showing the stacking of corrugated sheets along **b**. Perfect cleavage on (010) results from relatively weak bonding between structural sheets.

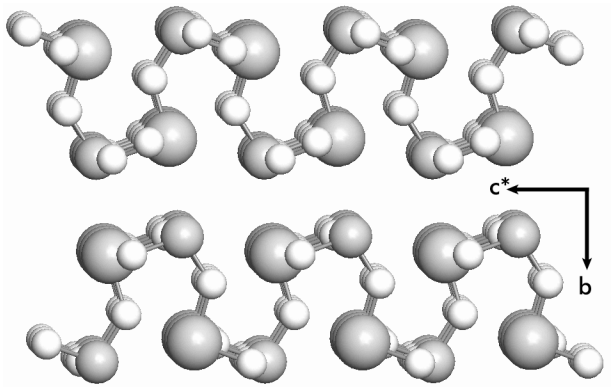

FIGURE 2. Long range bonding scheme within a single corrugated sheet of the Sb_claudetite structure. The lower drawing shows a single sheet viewed down **a**, with the Sb-O1 interaction at 2.947 Å, which is perpendicular to the direction of corrugation. The upper the drawing shows chains of ...-O-As-O-Sb-... viewed down **b**, which is a 90º rotation on **c*** from the lower drawing. Two long range interactions between As-O2 at 2.903 Å and Sb-O3 at 2.791 Å occur along the ridges of the corrugations, and run subparallel to **a**.

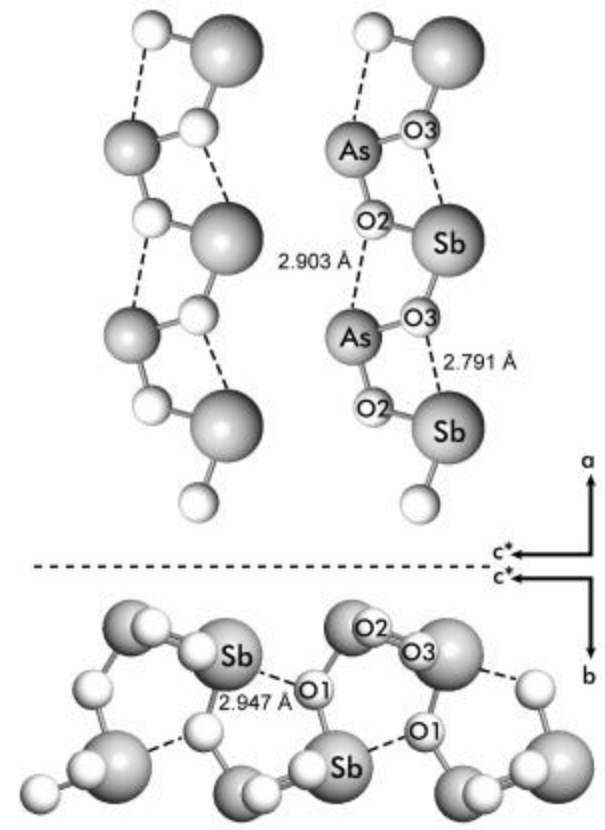

FIGURE 3. A projection down **c** of the crystal structure of Sb_claudetite showing the bonding scheme between layers. Two inter-layer bonds, Sb-O2 at 3.237 Å and As-O3 at 3.346 Å, hold the sheets together. The electron densities at the critical points of these bonds rank as the lowest among all of the bcp found by quantum calculations (Table 6), and result in cleavage along (010).